508 | Juli 1990

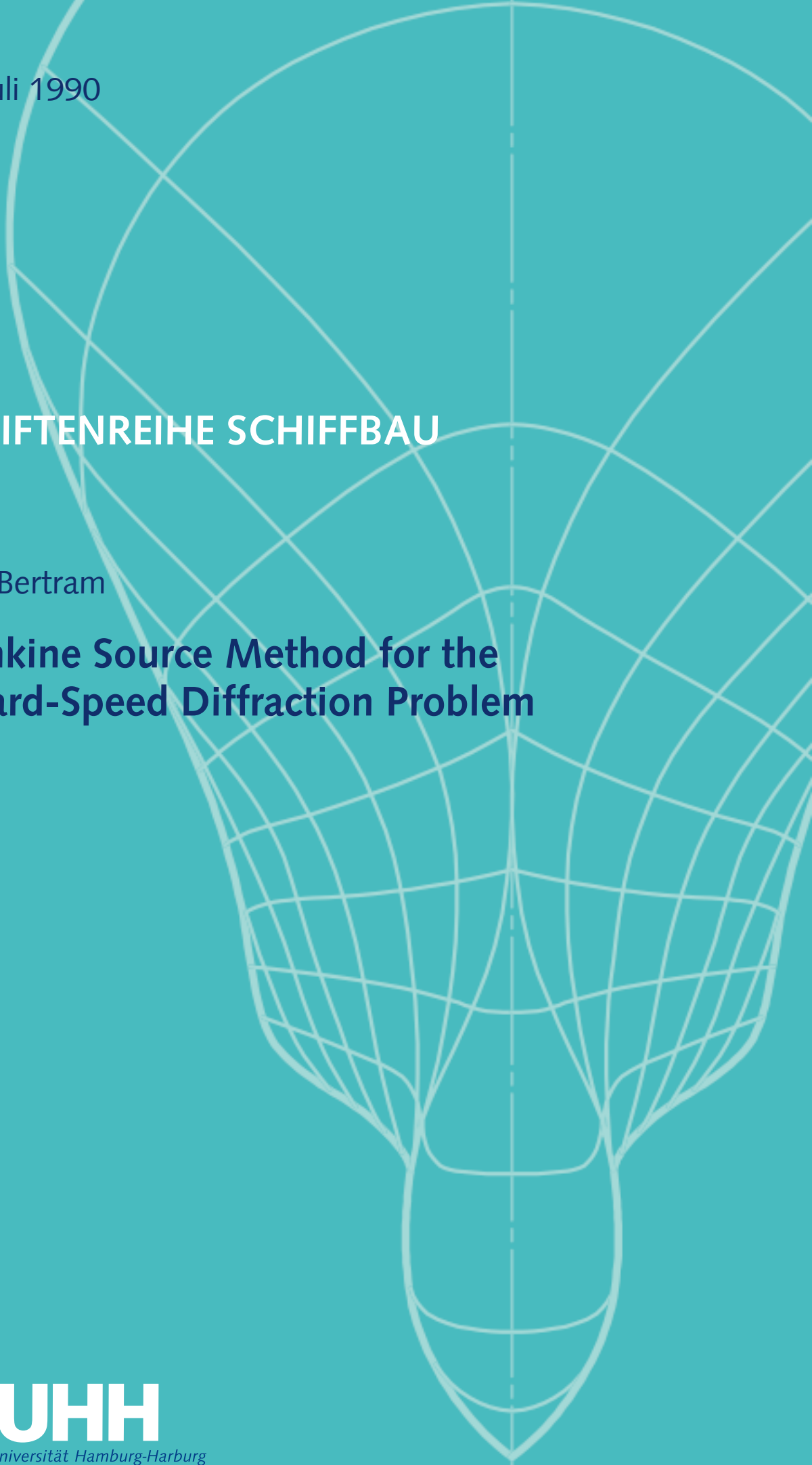

SCHRIFTENREIHE SCHIFFBAU

Volker Bertram

A Rankine Source Method for the Forward-Speed Diffraction Problem

TUHH
Technische Universität Hamburg-Harburg

A Rankine Source Method for the Forward-Speed Diffraction Problem

Volker Bertram, Hamburg, Technische Universität Hamburg-Harburg, 1990

Schriftenreihe Schiffbau
Schwarzenbergstraße 95c
D-21073 Hamburg

http://www.tuhh.de/vss

INSTITUT FÜR SCHIFFBAU DER UNIVERSITÄT HAMBURG

Bericht Nr. 508

A RANKINE SOURCE METHOD FOR THE FORWARD-SPEED DIFFRACTION PROBLEM

von

Volker Bertram

Juli 1990

Abstract

The forward-speed diffraction problem for $\tau = \omega_e U/g > 0.25$ in harmonic waves of small amplitude is solved using Rankine sources. The stationary part of the potential is determined numerically meeting the nonlinear free surface condition. Radiation and open-boundary conditions are enapplied to a submerged spheroid and a Series 60 ship ($C_B = 0.7$). Results agree well with other methods and experiments. But similar results are obtained using uniform flow as an approximation for the stationary part of the flow.

Table of contents

List of figures

1. State of the art

A ship with smooth surface moves with uniform speed U in a homogeneous, incompressible and inviscous fluid, which is only bounded by the ship's hull and the free surface. The flow is irrotational. The velocity field for such an ideal fluid can be described by one scalar quantity, namely the potential function $\phi(x, y, z, t)$. The velocity component of the flow in arbitrary direction relative to an inertial system x, y, z (described in Chapter 3.) is given by the partial derivative of the potential with respect to this direction. The influence of a harmonic incident wave of small amplitude h, coming from arbitrary direction, is investigated. For a reduced frequency $\tau = U\omega_e/g > 0.25$ diffracted waves can not propagate ahead of of the ship. Only such cases are considered here. The hull shape is assumed to be symmetric to its center line.

The traditional way to calculate wave-induced forces on ships is strip theory. In essence strip theory treats a three-dimensional body as hydrodynamically independent two-dimensional sections. The numerical computations of the flow about these independent sections are quite simple. The principal features of the strip theory were already set forth in the landmark paper by *Korvin-Kroukovsky (1955)* and improved two years later by *Korvin-Kroukovsky and Jacobs (1957)*. At present the standard strip-theory most often cited is that of *Salvesen, Tuck and Faltinsen (1970)*. The same basic approach is followed in most other strip theories, which differ mainly in their choice of the method for solving the two-dimensional subproblems by e.g. by describing a cross section by a Lewis transformation, close-fit methods, etc. *Faltinsen (1987)* estimates that the limit of applicability for high speeds is reached at a Froude number F_n of approximately 0.4.

Newman (1978) and *Sclavounos (1984)* developed the unified slender-body theory as a replacement for the strip theory. Slenderness was used as a justification to apply a quasi two-dimensional inner flow near the hull and a complementary three-dimensional outer flow generated by sources on the longitudinal axis of the ship. While featuring a better theoretical foundation than strip methods, the unified theory failed to show significant improvements of results in comparison with experiments.

Yeung and Kim (1981) presented another alternative to strip theory. The oscillatory flow is viewed from a cross-flow plane fixed in space as a transient two-dimensional disturbance caused by the oscillating motion of a slender ship passing through.

Lee (1983) developed a finite-difference method to calculate the added resistance in head waves. It is only valid for short wave lengths. An extension to wave lengths which produce reflected waves ahead of the ship is not possible.

Schulze (1969), *Chang (1980)* and *Inglis and Price (1981)* attempted fully three-dimensional numerical solutions. All these methods use a similar approach. The flow potential is divided into a stationary part and an instationary part, which is assumed to be small. For the stationary part, the crudest possible approximation, uniform flow of ship speed U, is chosen neglecting the influence of the additional local steady flow around the ship in smooth water. Havelock sources fulfilling the resulting linearized free-surface condition are distributed on the hull or the centerplane of the ship. The involved Green functions are very difficult to evaluate numerically. Evident in all three studies is a need for finer discretization of body geometry.

The above mentioned methods determine solutions in the frequency domain. In the recent past time-domain methods have been developed at the University of Michigan by *Liapis and Beck (1985)*, *Liapis (1986)* and *King(1987)*. *Beck and Magee (1988)* give a compendium of the results. These methods also approximate the steady flow by a uniform flow. In many cases the results agree better with experiments than the results of strip theory. *King (1987)* suspects that in some problematic cases the linearization of the free-surface condition might be too crude.

Nakos and Sclavounos (1989,1990) applied their Rankine source method to steady and time-harmonic free-surface flows. Rankine sources involve very simple Green functions $(1/r)$ for the potential fulfilling only the governing differential equation (Laplace's equation) and a condition of decay towards infinity. For free-surface problems, both hull surface and water surface must be discretized to fulfill the respective boundary conditions in a collocation scheme. Nakos and Sclavounos' stability analysis of Rankine source methods yields general guidelines for "proper" discretization of the free surface. For $\tau > 0.25$ good agreement with analytical results for an oscillating source is obtained. The wave pattern for a heaving Wigley hull shape is plausible. The open boundary condition at the outer border of the discretized part of the free surface is met in analogy to the steady flow problem by a special quadratic-splines approximation, *Sclavounos and Nakos (1988)*.

None of the foregoing theories properly accounts for the interaction between the steady wave system and the incident wave. Like Nakos and Sclavounos, I shall use a Rankine source method, which already has been found to be successful for determining the steady wave resistance in smooth water *(Jensen et al. (1986), Jensen (1988), Jensen et al. (1989))*. However, the stationary part of the flow will not be set to uniform parallel flow, but is determined numerically as by *Jensen et al. (1989)*. (The applicability of this method is limited to Froude numbers $0.2 < F_n < 0.4$ and ships of moderate flare in the water line at rest.) The potential of the incident wave of small amplitude h is known explicitly. Simple Rankine-type singularity distributions approximate the remaining instationary flow. Singularities are distributed on the hull surface and above the free surface. While for the steady flow around a ship in smooth water time-independent source strengths are chosen, harmonically oscillating source strengths are necessary for the wave-induced flow. Suitable source strengths for fulfilling the boundary conditions of the oscillating portion of the flow are determined in a collocation method. Radiation condition and "open boundary"-condition – avoiding unwanted reflections at the artificial boundary of the computational domain – are enforced numerically by a technique developed by *Jensen et al. (1986)*, *Jensen (1988)* and *Bertram (1990)*.

2. Nomenclature

A	area
$\vec{a}$	particle acceleration
$\vec{a}^g$	acceleration as def. in (14)
B	auxiliary variable as def. in (31), breadth
c	celerity of waves
d	depth of submergence
$\vec{d}$	differentiation vector for incident wave
D	diameter
$\vec{F}$	force vector
F_n	Froude number ($F_n = U/\sqrt{gL}$)
g	gravity acceleration ($g = 9.81 m/s^2$)
h	wave amplitude
i	$\sqrt{-1}$
k	wave number
L	length of body/ship
$\vec{M}$	vector of moments
$\vec{n}$	inward normal unit vector
p	pressure
p_0	atmospheric pressure
S	wetted surface of hull
T	draft
U	speed of ship
$\vec{x}$	coordinate vector with components x, y, z
x, y, z	coordinates of inertial system
x', y', z'	coordinates of system fixed in space

ε	phase of complex number
ζ	z-coordinate of free surface
λ	wave length
μ	angle of encounter
ρ	density of water
σ	source strength
τ	reduced frequency $U\omega_e/g$
ϕ	velocity potential
ψ	elementary potential of unit source strength
ω	wave frequency
ω_e	frequency of encounter

Δ	Laplace operator
∇	volume displacement, Nabla-operator
Re	real part of complex variable

superscripts

a	antimetrical
d	diffraction
e	exciting
fk	Froude-Krilov
nk	Neumann-Kelvin
s	symmetrical
t	total
w	incident wave
(i)	of order i
i	of order 1 without incident wave
$\hat{}$	complex amplitude

subscripts

c	collocation point
i	point index, element index
j	point index, element index
s	source
t	partial time-derivative
x, y, z	partial derivatives
$1, 2, 3$	component of vector

Quantities are given in the SI-system of units. Additional symbols are defined as they appear in the text. RSM stands for Rankine source method.

3. Coordinate systems

1) Coordinate system fixed in space O', x', y', z'

This is a right-handed Cartesian coordinate system. x' points in the direction of progress of the incident wave. z' points vertically downward. O' lies in the undisturbed free surface.
The angle of encounter between ship and incident wave is defined in this coordinate system as depicted:

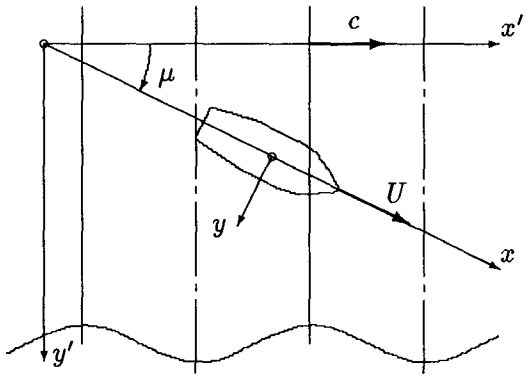

Fig.3.1: Angle of encounter μ

2) Inertial coordinate system O, x, y, z

The right-handed Cartesian coordinate system moves uniformly with velocity U. x points forwards, z vertically downwards.

The ship encounters forces (and moments) which are periodic in time with frequency of encounter ω_e. The components of the force vector $\vec{F}$ and the moment vector $\vec{M}$ are denoted:

F_1 force in x-direction
F_2 force in y-direction
F_3 force in z-direction

M_1 moment about x-axis
M_2 moment about y-axis
M_3 moment about z-axis

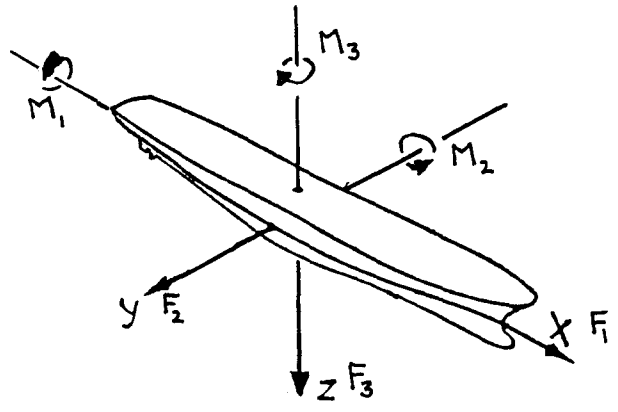

Fig.3.2: Inertial coordinate system

The relation between the $Oxyz$-system (inertial) and the $O'x'y'z'$-system (fixed in space) is:

$$x' = (x + Ut)\cos\mu - y\sin\mu \quad (1)$$
$$y' = (x + Ut)\sin\mu + y\cos\mu \quad (2)$$
$$z' = z \quad (3)$$

4. Determination of the potential

4.1. Physical description of the problem

For the assumed potential flow, conservation of mass and incompressibility give the Laplace equation, which must hold in the whole fluid domain:

$$\Delta\phi^t = 0 \tag{4}$$

On the boundaries of the fluid domain the following conditions must be met:

- constant (atmospheric) pressure at the free surface
- no water flows through the free surface
- no water flows through the ship's hull
- no water flows through the sea bottom (which is at infinite depth)
- diffraction waves must propagate out of the computational domain
- for $\tau > 0.25$ diffraction waves may not propagate ahead of the ship

The boundary conditions will be discussed more closely in the following chapters.

4.2. Perturbation approach for a first-order theory

A perturbation formulation for the potential is used:

$$\phi^t = \phi^{(0)} + \phi^{(1)} + \phi^{(2)} + ... \tag{5}$$

$\phi^{(0)}$ is the part of the potential which is independent of the wave amplitude h. It is the solution of the stationary wave resistance problem. $\phi^{(1)}$ is proportional to h, $\phi^{(2)}$ proportional to h^2, etc. Since I assume the wave amplitude h to be small, I will truncate the above series. Within a first-order theory (linearized theory) terms proportional to h^2 or higher powers of h will be neglected. For simplicity the equality sign is used here to denote equality of low-order terms only, i.e. $A = B$ means $A = B + O(h^2)$.

I describe both the z-component of the free surface ζ and the potential in a first-order formulation:

$$\phi^t(x,y,z;t) = \phi^{(0)}(x,y,z) + \phi^{(1)}(x,y,z;t) \tag{6}$$

$$\zeta^t(x,y;t) = \zeta^{(0)}(x,y) + \zeta^{(1)}(x,y;t) \tag{7}$$

$\phi^{(1)}$ and $\zeta^{(1)}$ are time harmonic with ω_e, the frequency of encounter:

$$\phi^{(1)}(x,y,z;t) = Re(\hat{\phi}^{(1)}(x,y,z)\, e^{i\omega_e t}) \tag{8}$$

$$\zeta^{(1)}(x,y;t) = Re(\hat{\zeta}^{(1)}(x,y)\, e^{i\omega_e t}) \tag{9}$$

Correspondingly the symbol $\hat{}$ is used to designate the complex amplitude of all other first-order quantities time periodic with ω_e, such as forces, pressures, etc.
Within a linearized theory the superposition principle can be used. The total solution is a linear combination of the solutions for each independent problem.

The instationary potential $\phi^{(1)}$ is divided into the potential of the incident wave ϕ^w and the diffraction potential ϕ^d:

$$\phi^{(1)} = \phi^w + \phi^d \tag{10}$$

It is convenient to divide ϕ^w and ϕ^d into symmetrical and antimetrical parts to take advantage of the ship's symmetry:

$$\begin{aligned} \phi^w(x,y,z) &= \underbrace{\frac{\phi^w(x,y,z)+\phi^w(x,-y,z)}{2}}_{\phi^{w,s}(x,y,z)} + \underbrace{\frac{\phi^w(x,y,z)-\phi^w(x,-y,z)}{2}}_{\phi^{w,a}(x,y,z)} \\ \phi^d &= \phi^{d,s} + \phi^{d,a} \end{aligned} \tag{11}$$

4.3. Potential of the stationary flow

A deduction of the boundary conditions of the stationary flow can be found in *Jensen (1988)* or *Jensen et al. (1989)*. So here the formulae are given without detailed comment.

In the whole fluid domain Laplace's equation holds:

$$\Delta\phi^{(0)} = 0 \tag{12}$$

The particle acceleration in the stationary flow is:

$$\vec{a}^{(0)} = (\nabla\phi^{(0)}\nabla)\nabla\phi^{(0)} \tag{13}$$

I define an acceleration vector $\vec{a}^g$:

$$\vec{a}^g \stackrel{\text{def}}{=} (\nabla\phi^{(0)}\nabla)\nabla\phi^{(0)} - g\nabla z \tag{14}$$

On the ship hull ($S(\vec{x}) = 0$):

$$\vec{n}\nabla\phi^{(0)} = 0 \tag{15}$$

At the stationary free surface ($z = \zeta^{(0)}$):

$$\nabla\phi^{(0)}\vec{a}^g = 0 \tag{16}$$

$$\frac{1}{2}(\nabla\phi^{(0)})^2 - g\zeta^{(0)} = \frac{1}{2}U^2 \tag{17}$$

The surface height $\zeta^{(0)}$ can be eliminated from (16) and (17); at $z = \zeta^{(0)}$:

$$\frac{1}{2}\nabla\phi^{(0)}\nabla(\nabla\phi^{(0)})^2 - g\phi_z^{(0)} = 0 \tag{18}$$

In the Neumann-Kelvin problem, this non-linear free-surface condition is linearized using uniform flow as an approximation:

$$U^2\phi_{xx}^{(0)} - g\phi_z^{(0)} = 0 \qquad \text{at } z = 0 \tag{19}$$

Far away from the ship there are no steady waves, as $\phi^{(0)}$ becomes the potential of an undisturbed uniform parallel flow.

4.4. Potential of the incident wave

At the time $t = 0$ the incident wave has a trough at the coordinate origin:

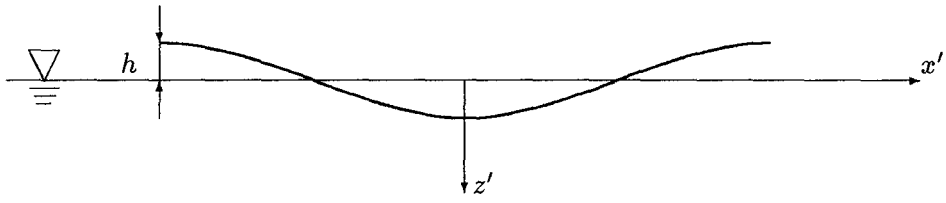

Fig.4.1: Incident wave at $t = 0$

The linearized potential of the incident wave, *Wehausen and Laitone (1960)*, on water of infinite depth is:

$$\phi^w = Re(-\frac{igh}{\omega}\, e^{-kz'}\, e^{i(\omega t - kx')}) \tag{20}$$

where k is the wave number and ω the frequency of the incident wave.

The frequency ω is coupled with the wave number k by:

$$\omega = \sqrt{gk} \tag{21}$$

The potential transforms into the inertial coordinate system:

$$\phi^w = Re(\underbrace{-\frac{igh}{\omega}\, e^{\vec{d}\vec{x}}}_{\hat{\phi}^w}\, e^{i\omega_e t}) \tag{22}$$

with ω_e as frequency of encounter:

$$\omega_e = \omega - k\, U \cos\mu \tag{23}$$

and $\vec{d}$:

$$\vec{d} = \begin{Bmatrix} -ik\cos\mu \\ ik\sin\mu \\ -k \end{Bmatrix} \tag{24}$$

As it is easily seen, the velocity corresponding to this potential is:

$$\nabla\phi^w = Re\left(\vec{d}\,\hat{\phi}^w\, e^{i\omega_e t}\right) \tag{25}$$

Note: $\hat{\phi}^w_y = d_2\hat{\phi}^w$, but $\hat{\phi}^{w,s} = d_2\hat{\phi}^{w,a}$ and $\hat{\phi}^{w,a} = d_2\hat{\phi}^{w,s}$.

4.5. Boundary condition at the free surface

At the free surface ($z = \zeta^t$) the pressure is constant, namely atmospheric pressure ($p = p_0$):

$$\frac{D(p - p_0)}{Dt} = 0 \tag{26}$$

where $\frac{D}{Dt}$ denotes the substantial derivative with respect to the time: $\frac{D}{Dt} = \frac{\partial}{\partial t} + (\nabla\phi^t\nabla)$.

The three conservation-of-momentum equations (Euler's equations) reduce by integration to Bernoulli's equation, giving at the free surface ($z = \zeta^t$) the dynamic boundary-condition:

$$\phi_t^t + \frac{1}{2}(\nabla\phi^t)^2 - g\zeta^t + \frac{p}{\rho} = \frac{1}{2}U^2 + \frac{p_0}{\rho} \tag{27}$$

No water flows through the free surface. This gives the kinematic boundary-condition at $z = \zeta^t$:

$$\frac{D\zeta^t}{Dt} = \phi_z^t \tag{28}$$

Combining (26) - (28) yields at $z = \zeta^t$:

$$\phi_{tt}^t + 2\nabla\phi^t\nabla\phi_t^t + \nabla\phi^t\nabla(\frac{1}{2}(\nabla\phi^t)^2) - g\phi_z^t = 0 \tag{29}$$

Formulating this condition in $\phi^{(0)}$ and $\phi^{(1)}$ and linearizing with regard to instationary terms gives at $z = \zeta^t$:

$$\phi_{tt}^{(1)} + 2\nabla\phi^{(0)}\nabla\phi_t^{(1)} + \nabla\phi^{(0)}\nabla\left(\frac{1}{2}(\nabla\phi^{(0)})^2 + \nabla\phi^{(1)}\nabla\phi^{(0)}\right) + \nabla\phi^{(1)}\nabla(\frac{1}{2}\left(\nabla\phi^{(0)}\right)^2) - g\phi_z^{(0)} - g\phi_z^{(1)} = 0 \tag{30}$$

Recall that $\vec{a}^{(0)} = (\nabla\phi^{(0)}\nabla)\nabla\phi^{(0)}$ is the stationary particle acceleration. It is convenient to introduce an abbreviation (compare *Jensen (1988)*, eq.(4-15)):

$$B = -\frac{1}{a_3^g}\frac{\partial}{\partial z}(\nabla\phi^{(0)}\vec{a}^g) \tag{31}$$

Eq. (30) is developed in a Taylor expansion around $\zeta^{(0)}$. Linearizing again with regard to instationary terms gives at $z = \zeta^{(0)}$:

$$\phi_{tt}^{(1)} + 2\nabla\phi^{(0)}\nabla\phi_t^{(1)} + \nabla\phi^{(0)}\vec{a}^g + \nabla\phi^{(0)}(\nabla\phi^{(0)}\nabla)\nabla\phi^{(1)} + \nabla\phi^{(1)}(\vec{a}^{(0)} + \vec{a}^g) - Ba_3^g\zeta^{(1)} = 0 \tag{32}$$

This boundary condition must be fulfilled at any time. The stationary terms give (16). For the instationary terms the time derivations are performed:

$$-\omega_e^2\hat{\phi}^{(1)} + 2i\omega_e\nabla\phi^{(0)}\nabla\hat{\phi}^{(1)} + \nabla\phi^{(0)}(\nabla\phi^{(0)}\nabla)\nabla\hat{\phi}^{(1)} + \nabla\hat{\phi}^{(1)}(\vec{a}^{(0)} + \vec{a}^g) - Ba_3^g\hat{\zeta}^{(1)} = 0 \tag{33}$$

$\hat{\zeta}^{(1)}$ will be substituted by an expression depending solely on $\zeta^{(0)}$, $\phi^{(0)}(\zeta^{(0)})$ and $\hat{\phi}^{(1)}(\zeta^{(0)})$. To this end, Bernoulli's equation (27) is also developed in a Taylor expansion.

Bernoulli's equation at $z = \zeta^{(0)} + \zeta^{(1)}$:

$$\phi_t^{(1)} + \frac{1}{2}(\nabla\phi^t)^2 - gz = \frac{1}{2}U^2 \tag{34}$$

Truncated Taylor expansion gives at $z = \zeta^{(0)}$:

$$\phi_t^{(1)} + \frac{1}{2}(\nabla\phi^t)^2 - g\zeta^{(0)} - \frac{1}{2}U^2 + \left(\nabla\phi^t\nabla\phi_z^t - g\right)\zeta^{(1)} = 0 \tag{35}$$

This equation holds at any time. The stationary terms give (17). For the instationary terms the time derivations are performed, giving at $z = \zeta^{(0)}$:

$$\hat{\zeta}^{(1)} = -\frac{i\omega_e\hat{\phi}^{(1)} + \nabla\phi^{(0)}\nabla\hat{\phi}^{(1)}}{a_3^g} \tag{36}$$

By inserting this expression in (33), the free-surface condition at $z = \zeta^{(0)}$ becomes:

$$(-\omega_e^2 + Bi\omega_e)\hat{\phi}^{(1)} + \left((2i\omega_e + B)\nabla\phi^{(0)} + \vec{a}^{(0)} + \vec{a}^g\right)\nabla\hat{\phi}^{(1)} + \nabla\phi^{(0)}(\nabla\phi^{(0)}\nabla)\nabla\hat{\phi}^{(1)} = 0 \tag{37}$$

For cruder models of the stationary flow, this free-surface condition simplifies. If the stationary flow is set to uniform flow, (37) gives at $z = 0$:

$$(U\frac{\partial}{\partial x} - i\omega_e)^2\hat{\phi}^{(1)} - g\hat{\phi}_z^{(1)} = 0 \tag{38}$$

For zero speed, (37) becomes the well-known condition:

$$\omega^2\hat{\phi}^{(1)} + g\hat{\phi}_z^{(1)} = 0 \tag{39}$$

4.6. Boundary condition at the ship hull

A point on the ship's hull shall be given by $S(\vec{x}) = 0$. $\vec{n}$ is the normal unit vector pointing into the hull. Water does not penetrate the ship's hull. This condition is expressed at $S(\vec{x}) = 0$:

$$\vec{n}\nabla\hat{\phi}^{(1)} = 0 \tag{40}$$

4.7. Final hull and free-surface boundary conditions

In (6) and (10) the total velocity potential was decomposed:

$$\phi^t = \phi^{(0)} + Re\left((\hat{\phi}^{w,s} + \hat{\phi}^{w,a} + \hat{\phi}^{d,s} + \hat{\phi}^{d,a})\, e^{i\omega_e t}\right) \tag{41}$$

The symmetrical and antimetrical diffraction problems are formulated separately. Both $\phi^{d,s}$ and $\phi^{d,a}$ must independently fulfill Laplace's equation (4) and vanish at infinity.

The boundary conditions on the hull and the free surface are given explicitly for the symmetrical case. The same conditions must hold for the antimetrical case where s is substituted by a.

boundary condition at $S(\vec{x}) = 0$
$\vec{n}\nabla\hat{\phi}^{d,s} + \vec{n}\nabla\hat{\phi}^{w,s} = 0$

boundary condition at $z = \zeta^{(0)}$
$(-\omega_e^2 + Bi\omega_e)\hat{\phi}^{d,s} + \left((2i\omega_e + B)\nabla\phi^{(0)} + \vec{a}^{(0)} + \vec{a}^g\right)\nabla\hat{\phi}^{d,s} + \nabla\phi^{(0)}(\nabla\phi^{(0)}\nabla)\nabla\hat{\phi}^{d,s} +$
$+(-\omega_e^2 + Bi\omega_e)\hat{\phi}^{w,s} + \left((2i\omega_e + B)\nabla\phi^{(0)} + \vec{a}^{(0)} + \vec{a}^g\right)\nabla\hat{\phi}^{w,s} + \nabla\phi^{(0)}(\nabla\phi^{(0)}\nabla)\nabla\hat{\phi}^{w,s} = 0$

Note: $\hat{\phi}_y^{w,s} = d_2\hat{\phi}^{w,a}$, $\hat{\phi}_{xy}^{w,s} = d_1d_2\hat{\phi}^{w,a}$, $\hat{\phi}_{yz}^{w,s} = d_2d_3\hat{\phi}^{w,a}$

5. Determination of exciting forces

The forces $\vec{F}$ and moments $\vec{M}$ acting on the ship result from integrating the pressure over the instantaneous wetted surface. The pressure expression $p-p_0$ is zero at the free surface. Therefore, within first-order accuracy, the instantaneous wetted surface can be replaced by the mean wetted surface S:

$$\vec{F} = \int_S (p - p_0)\vec{n}\ dS \tag{42}$$

$$\vec{M} = \int_S (p - p_0)(\vec{x} \times \vec{n})\ dS \tag{43}$$

The pressure is given by Bernoulli's equation:

$$p - p_0 = -\rho\left(\phi_t^t + \frac{1}{2}(\nabla\phi^t)^2 - \frac{1}{2}U^2 - gz\right) \tag{44}$$

$$= -\rho\left(\phi_t^{(1)} + \frac{1}{2}(\nabla\phi^{(0)})^2 + \nabla\phi^{(0)}\nabla\phi^{(1)} - \frac{1}{2}U^2 - gz\right) \tag{45}$$

The pressure is divided into a stationary and an instationary part:

$$p - p_0 = p^{(0)} + p^{(1)} \tag{46}$$

where

$$p^{(0)} = -\rho\left(\frac{1}{2}(\nabla\phi^{(0)})^2 - \frac{1}{2}U^2 - gz\right) \tag{47}$$

$$p^{(1)} = -\rho\left(\phi_t^{(1)} + \nabla\phi^{(0)}\nabla\phi^{(1)}\right) \tag{48}$$

The first-order (exciting) periodic forces and moments are:

$$\vec{F}^e = \int_S p^{(1)}\vec{n}\ dS \tag{49}$$

$$\vec{M}^e = \int_S p^{(1)}(\vec{x} \times \vec{n})\ dS \tag{50}$$

The Froude-Krilov forces and moments are obtained integrating only the pressure induced by the undisturbed wave:

$$\vec{F}^{fk} = \int_S -\rho(\phi_t^w - U\phi_x)\vec{n}\ dS \tag{51}$$

$$\vec{M}^{fk} = \int_S -\rho(\phi_t^w - U\phi_x)(\vec{x} \times \vec{n})\ dS \tag{52}$$

6. Discretization

The unknown parts of the potential, $\hat{\phi}^{d,s}$ and $\hat{\phi}^{d,a}$, are approximated as superpositions of potentials ψ_i of a (finite) number of Rankine-type singularities:

$$\hat{\phi}^{d,s} = \sum_i \hat{\sigma}_i^{d,s} \psi_i \qquad \hat{\phi}^{d,a} = \sum_i \hat{\sigma}_i^{d,a} \psi_i \tag{53}$$

where $\hat{\sigma}_i$ denotes a so far unknown source strength.

Each potential ψ_i fulfills a priori Laplace's equation and decays towards infinity. Ship and water surface are represented by a (finite) number of discrete points (collocation points) at which the respective boundary conditions of chapter 4.7 are fulfilled in a collocation scheme. The number of collocation points is equal to the number of unknown source strengths. Thus the symmetrical resp. antimetrical problem forms a system of linear equations.

The singularities (panels) are distributed on the following surfaces (numbers correspond to the figure below):

1 - starboard part of the ship's hull up to a plane parallel to the still water line above the stationary waterline
2 - a mirror image of surface 1 plane of reflection is above mentioned plane parallel to the still water line
3 - a horizontal plane above the stationary water surface
4 - mirror images of surfaces 1 to 3 at the midship plane (x-z-plane)

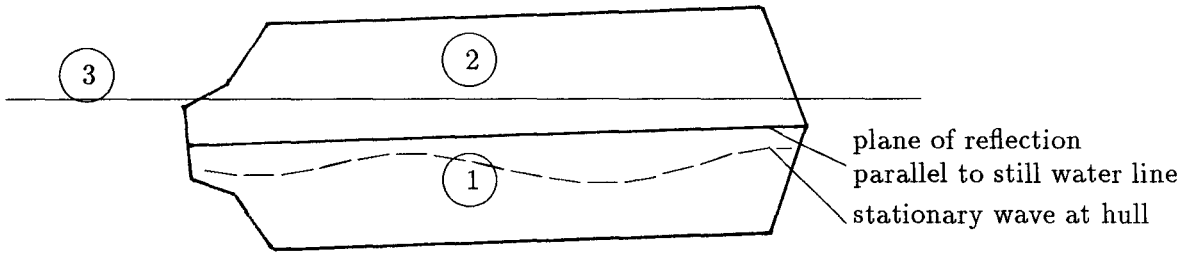

Fig.6.1: Starboard view of surfaces with singularities

The source strengths of the panels on surfaces 2 and 4 are set to be equal in absolute value to their corresponding "original" panels. They also have same sign except on surface 4 for the antimetrical cases.

Thus only the distribution of source strength on the starboard side (surfaces 1 and 3) remains to be determined. If the resulting flow is relatively smooth the boundary conditions will be approximately met also between the collocation points.

6.1. Discretization of ship

For the ship special panels developed by *Jensen (1988)* are used. Each panel of constant source strength consists of triangles clustered around the collocation point forming thus a (usually non-plane) polygon. Generally polygons with 3 or 4 sides are used. To avoid evaluation of transcendental functions typically involved with Rankine-type panels (*Hess and Smith (1964)*, *Webster (1975)*, *Yeung and Bai (1974)*), simple numerical integration is used. For the collocation point lying within the panel the singularities in the involved integrals are reduced by adding a tangential sphere of constant source strength. For all collocation points lying not within the panel, its effect

is approximated by a simple Rankine point-source. On the ship the collocation points lie (roughly) in the middle of the panels.

Forces and moments on the hull are evaluated by pressure integration. The pressure at the collocation point is taken to be constant over the panel. The mean wetted area of the panel is determined as by *Jensen (1988)*: The velocity at the collocation point corresponds to a surface elevation. Only the area of the panel lying below this elevation is used for integration.

6.1.1. Potential

For calculating the periodic pressures on the ship surface, the potential has to be evaluated there. The potential in a collocation point $\vec{x}_c$ is represented by a Rankine-source distribution:

$$\phi(\vec{x}_c) = \int_S \sigma(\vec{x}_s)\, \mathcal{G}(\vec{x}_s, \vec{x}_c)\, dS \tag{54}$$

$\mathcal{G}$ is the Green function of a source of unit strength:

$$\mathcal{G}(\vec{x}_s, \vec{x}_c) = \frac{-1}{4\pi} \frac{1}{|\vec{x}_s - \vec{x}_c|} \tag{55}$$

The surface S consists of the body surface S_B (surfaces 1, 2 and mirror images 4) and the water surface S_W (surface 3 and mirror images 4). First the integral over S_B is considered. Discretization into panels transforms the integral into a sum of N_B panels of source strengths σ_s:

$$\phi(\vec{x}_c) = \sum_{s=1}^{N_B} \sigma_s\, G(\vec{x}_s, \vec{x}_c) \tag{56}$$

The Green function G is the integral of $\mathcal{G}$ over one panel. If $c = s$, i.e. the collocation point lies within the panel, this integral is evaluated analytically. The panel is divided into N_t plane triangles:

$$G = \sum_{j=1}^{N_t} G_j \tag{57}$$

The integral over one triangle, G_j, leads to a relatively simple expression. Let the collocation point be at the upper corner of the triangle. Using a local coordinate system, the geometrical properties of any triangle can be described as depicted.

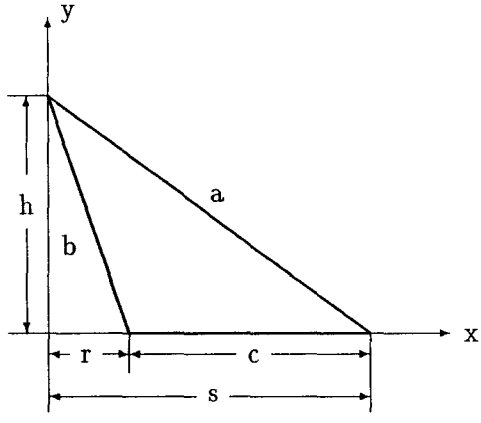

The potential at the upper corner point is then given by:

$$G_j = \frac{-1}{4\pi} \int_{y=0}^{h} \int_{x=r(1-y/h)}^{s(1-y/h)} \frac{1}{\sqrt{x^2 + (h-y)^2}}\, dx\, dy \tag{58}$$

The integral over x is readily evaluated:

$$\int_{x=r(1-y/h)}^{s(1-y/h)} \frac{1}{\sqrt{x^2+(h-y)^2}}\,dx = \left[\ln\left(x+\sqrt{x^2+(h-y)^2}\right)\right]_{r(1-y/h)}^{s(1-y/h)} \tag{59}$$

$$= \ln\left(\frac{\frac{s}{h}+\sqrt{(1+(\frac{s}{h})^2)}}{\frac{r}{h}+\sqrt{(1+(\frac{r}{h})^2)}}\right) \tag{60}$$

$$= \ln(\frac{s+a}{r+b}) \tag{61}$$

$$= \ln(\frac{a^2-b^2+c^2+2ac}{a^2-b^2-c^2+2bc}) \tag{62}$$

$$= \ln(\frac{(a+b+c)(a-b+c)}{(a+b-c)(a-b+c)}) \tag{63}$$

$$= \ln(\frac{a+b+c}{a+b-c}) \tag{64}$$

This expression is independent of y. The integration over y then simply gives:

$$\phi_j = h\,\ln(\frac{a+b+c}{a+b-c}) \tag{65}$$

The area A_j of the triangle is given by:

$$A_j = \frac{1}{2}hc \tag{66}$$

The potential can then be written as:

$$G_j = -\frac{1}{4\pi}\frac{2A_j}{c}\,\ln(\frac{a+b+c}{a+b-c}) \tag{67}$$

This expression is independent of the local coordinate system. It is fast to evaluate on a computer and not sensitive to numerical errors.

For $c \neq s$, i.e. collocation points outside of the panel, the panel is substituted by a simple point source weighted by the panel area: $G = A_s\mathcal{G}$, where A_s is the sum over all N_t triangle areas A_j. The integral over S_W is also substituted by a sum of N_W single point sources weigthed by the panel area:

$$\phi(\vec{x}_c) = \sigma_c G(\vec{x}_s,\vec{x}_c) + \sum_{\substack{s=1\\ s\neq c}}^{N_B+N_W} \sigma_s A_s \mathcal{G}(\vec{x}_s,\vec{x}_c) \tag{68}$$

6.1.2. Velocities

Jensen (1988) gives a derivation for the first derivatives of the potential assuming a smooth surface. The main ideas are repeated here. We consider a point $\vec{x}_c$ on S_B. ∇_c denotes the Nabla-operator acting on $\vec{x}_c$. $\vec{n}$ is the normal vector at $\vec{x}_c$ pointing into the body, $\vec{s}$ and $\vec{t}$ are two orthogonal tangential vectors.

The normal velocity v_n is

$$v_n(\vec{x}_c) = \vec{n}(\vec{x}_c)\,\nabla_c\phi(\vec{x}_c) = \int_S \sigma(\vec{x}_s)\,\vec{n}(\vec{x}_c)\,\nabla_c\mathcal{G}(\vec{x}_s,\vec{x}_c)\,dS - \frac{1}{2}\sigma(\vec{x}_c) \tag{69}$$

In the integration surface S, the singularity at $\vec{x}_c = \vec{x}_s$ is excluded in an ε-perimeter. First we consider the integral over S_B.

As the choice of tangential vectors is rather arbitrary, only one component is considered here. The tangential velocity is:

$$v_t = \vec{t}\,\nabla_c\phi = \int_S \sigma(\vec{x}_s)\,\vec{t}(\vec{x}_c)\,\nabla_c\mathcal{G}(\vec{x}_s,\vec{x}_c)\,dS \tag{70}$$

The integrand in (69) tends to zero for $\vec{x}_s \to \vec{x}_c$ and numerical evaluation of the integral is straightforward. The integrand in (70) is singular for $\vec{x}_s \to \vec{x}_c$. Therefore the formulation for the tangential velocity is modified.

A sphere of constant source-strength distribution does not induce a tangential velocity on its surface:

$$\int_{S_S} \vec{t}(\vec{x}_c)\,\nabla_c\mathcal{G}(\vec{x}_s,\vec{x}_c)\,dS = 0 \tag{71}$$

Let the sphere touch the (closed) body surface S_B tangentially in $\vec{x}_c$, and let the shere's center $\vec{o}$ lie within the body. Then a projection ray from $\vec{o}$ through any point $\vec{k}$ on the sphere surface S_S gives at least one point $\vec{x}_c$ on the body surface S_B. Let $\vec{k} = P(\vec{x}_c)$ denote this mapping procedure. It projects body surface elements dS_B on sphere surface elements dS_S. Let r be the relative size of the surface elements: $dS_S = r\,dS_B$. r has the sign of the scalar product of the corresponding unit normal vectors on body and sphere surface. Then the following relation holds:

$$\int_{S_S} \vec{t}(\vec{x}_c)\,\nabla_c\mathcal{G}(\vec{k},\vec{x}_c)\,dS_S = \int_{S_B} \vec{t}(\vec{x}_c)\,\nabla_c\mathcal{G}(P(\vec{x}_s),\vec{x}_c)\,r\,dS_B = 0 \tag{72}$$

This second integral is multiplied by $\sigma(\vec{x}_c)$ and subtracted from (70):

$$v_t(\vec{x}_c) = \int_{S_B} [\sigma(\vec{x}_s)\vec{t}(\vec{x}_c)\,\nabla_c\mathcal{G}(\vec{x}_s,\vec{x}_c) - \sigma(\vec{x}_c)\vec{t}(\vec{x}_c)\,\nabla_c\mathcal{G}(P(\vec{x}_s),\vec{x}_c)\,r\,]\,dS \tag{73}$$

For $\vec{x}_s \to \vec{x}_c$, the integrand in (73) is still singular. However, within panels of constant source strength it tends to zero and the integral can be evaluated numerically.

The corresponding integrals over S_W do not contain a singularity. The integrands can be evaluated as (69) and (70).

The discretized formulations for v_n and v_t are:

$$v_n(\vec{x}_c) = -\frac{1}{2}\sigma_c + \sum_{\substack{s=1\\ s\neq c}}^{N_B+N_W} \sigma_s\vec{n}_c\nabla_c\mathcal{G}(\vec{x}_s,\vec{x}_c)A_s$$

$$v_t(\vec{x}_c) = \sum_{\substack{s=1\\ s\neq c}}^{N_B} \vec{t}_c[\sigma_s\nabla_c\mathcal{G}(\vec{x}_s,\vec{x}_c) - \sigma_c\nabla_c\mathcal{G}(P(\vec{x}_s),\vec{x}_c)\,r_k(\vec{x}_s)]A_s \tag{74}$$

$$+ \sum_{s=N_B+1}^{N_B+N_W} \vec{t}_c\sigma_s\nabla_c\mathcal{G}(\vec{x}_s,\vec{x}_c)A_s \tag{75}$$

The projection P of $\vec{x}_s$ on the tangential sphere of radius R and center $\vec{o} = \vec{x}_s + R\vec{n}$ is:

$$P(\vec{x}_s) = \frac{\vec{x}_s - \vec{o}}{|\vec{x}_s - \vec{o}|}R + \vec{o} \tag{76}$$

The relative size of area elements r is:

$$r(\vec{x}_s) = -\vec{n}\frac{\vec{x}_s - \vec{o}}{|\vec{x}_s - \vec{o}|}\left(\frac{R}{|\vec{x}_s - \vec{o}|}\right)^2 \tag{77}$$

Note that *Jensen (1988)* omitted the minus sign in the formula for r.

The transformation of the normal and tangential velocity components to the global system is straightforward:

$$\begin{Bmatrix} v_1 \\ v_2 \\ v_3 \end{Bmatrix} = \begin{bmatrix} n_1 & s_1 & t_1 \\ n_2 & s_2 & t_2 \\ n_3 & s_3 & t_3 \end{bmatrix} \begin{Bmatrix} v_n \\ v_s \\ v_t \end{Bmatrix} \tag{78}$$

6.2. Discretization of free surface

On the water surface the collocation points lie below the panels. The technique of separating the source surface from the water surface ("desingularization") is often viewed with some suspicion. However, it is admissable because of the smoothness, i.e. small curvature, of the water surface. It should be noted that the distance between the two surfaces (water/sources) is coupled to the grid spacing. In the (theoretical) limit of infinitesimal spacing, the two surfaces would coincide converging to the desired solution. *Cao et al. (1989)*, *Schultz et al. (1990)*, and *Cao et al. (1990)* confirmed in systematic numerical investigations of desingularization earlier experiences of its applicability, e.g. *Webster (1975)*, *Bertram and Jensen (1987)* and *Jensen (1988)*. The effect of a panel on the surface above the water surface on collocation points on the body or the water surface is generally approximated by a point source in the panel center. For "small" distances between panel and collocation point the panel is approximated by 4 point sources which are spaced 1/4 of the typical grid spacing in x- and y-direction around the panel center. *Jensen (1988)* used exclusively single point sources. He recommended twice the typical grid spacing for the height between still water line and source layer . Using the technique of several point sources for small distances, the height of the source layer can be reduced to one typical grid spacing. This improves the conditioning of the linear system of equation and thus the accuracy of the solution.

7. Radiation and open-boundary condition

Two problems have long impeded the application of Rankine-source methods (RSM) to free-surface flows:
1. The radiation condition: In the steady wave problem, waves will propagate only downstream; i.e. far ahead of the ship no waves may appear.
2. The open-boundary condition: Only a limited area of the free surface can be discretized. Waves must pass through the outer boundary of this area without significant reflection.

Both conditions must be fulfilled numerically in RSM. *Orlanski (1976)* lists various techniques for imposing the open-boundary condition numerically:

(1) Sommerfeld's radiation condition
(2) one-side differencing methods
(3) damping
(4) asymptotic matching

Orlanski derived for two-dimensional problems a non-linear boundary condition from Sommerfeld's condition. For three-dimensional problems Orlanski's condition gives a non-linear equation for every point where it is enforced. For the simple case of a heaving sphere of zero forward speed no solution for the resulting system of non-linear equations could be found if more than three points at the outer boundary were chosen. Orlanski's approach therefore seems to be inapplicable for the present problem.

Dawson (1977) was the first to present a practicable RSM method for the steady free-surface flow around a ship by developing a numerical technique for meeting radiation and open-boundary conditions. The radiation condition was enforced using a special four-point upstream finite-difference operator for calculating some of the derivatives in the free-surface condition. At the end of the free-surface grid two-point operators were used that served to dampen the waves. Dawson's method usually underpredicts the wave length by about 5% and shows some damping of the waves. Later variations of his method improved these shortcomings, e.g. *Sclavounos and Nakos (1988)* by using quadratic splines for deriving another finite-difference operator. Recently, *Nakos and Sclavounos (1990)* successfully applied their quadratic-spline scheme also to time-harmonic free-surface flows with reduced frequency $\tau > 0.25$.

Jensen (1988) showed the effectiveness of another numerical technique for the steady flow. By shifting the Rankine sources above the free surface versus the collocation points on the surface, both radiation and open-boundary condition are fulfilled. His trial computations for a submerged dipole show excellent agreement with analytical results. In analogy the applicability to time-harmonic problems is shown here for the example of a submerged point source moving steadily with speed U in an ideal fluid under a free surface. The source strength pulsates with unit amplitude and reduced frequency $\tau = U\omega/g$.

The surface $z = 0$ is discretized into a regular grid of $n_x \cdot n_y = N$ collocation points, (Fig.7.1). Δx and Δy denote the grid spacing in x- and y-direction. In a height h_s above the surface N Rankine point sources are located. For the sources the grid-spacing in x-direction is also Δx, in y-direction $\Delta\eta$. So sources are gradually shifted in y-direction reaching a maximum shift of ΔH at the outer boundary. All sources are shifted uniformly by $\Delta\Xi$ in x-direction. For small distances ($< 3\min(\Delta x, \Delta y)$ between source and collocation point, the single point source is substituted by 4 point sources of constant strength. The 4 sources form a rectangle of length $\Delta x/2$ and width $\Delta y/2$.

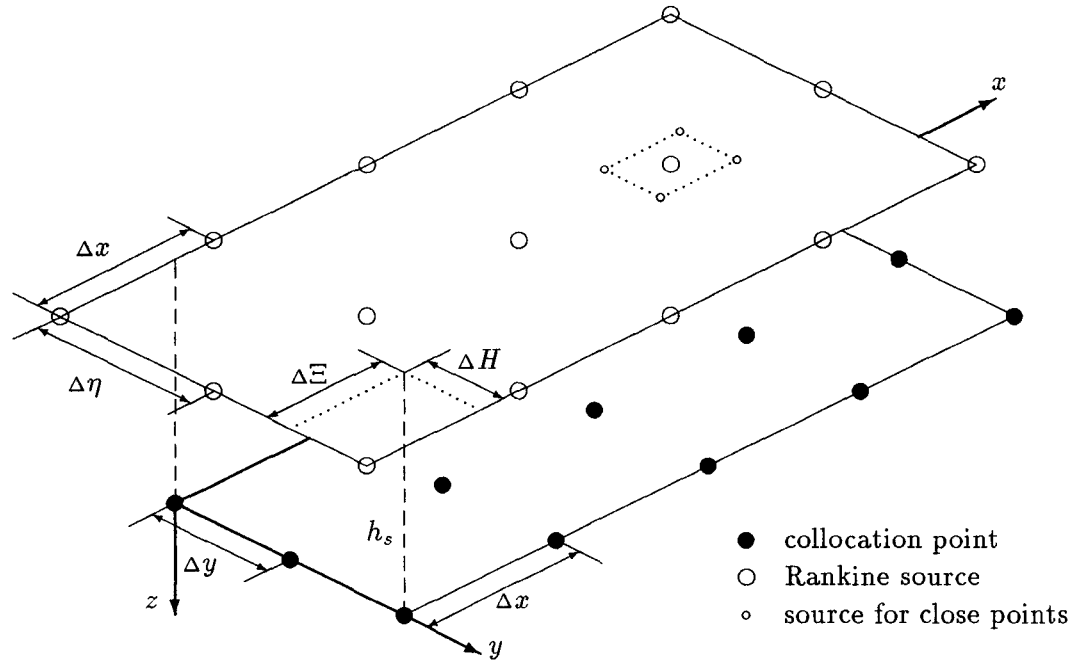

Fig.7.1: Rankine point sources are shifted relative to collocation points

The source strength σ_s of each source above the free surface pulsates with circular frequency ω: $\sigma_s = Re(\hat{\sigma}_s e^{i\omega t})$

Let $\vec{x}_d = (0, 0, d)$ be the location of the submerged pulsating source. The classical free-surface boundary condition (38) is discretized for each collocation point $\vec{x}_c$ forming a system of linear equations (SLE) for the unknown source strength amplitudes $\hat{\sigma}_s$:

$$\left(i\omega - U\frac{\partial}{\partial x}\right)^2 \mathcal{G}(\vec{x}_c, \vec{x}_d) - g\frac{\partial}{\partial z}\mathcal{G}(\vec{x}_c, \vec{x}_d)$$
$$+ \sum_{s=1}^{N} \hat{\sigma}_s \left(\left(i\omega - U\frac{\partial}{\partial x}\right)^2 \mathcal{G}(\vec{x}_c, \vec{x}_s) - g\frac{\partial}{\partial z}\mathcal{G}(\vec{x}_c, \vec{x}_s) \right) = 0 \qquad (79)$$

In numerical experiments for a submerged dipole, *Jensen (1988)* determined suitable values for $\Delta\Xi$ and ΔH for the steady wave problem ($\tau = 0$, $U > 0$), by finding maxima of $\ln|D|$, where D is the determinant of the SLE. He found maxima at $\Delta\Xi = 0$, $\Delta H = 0.2\Delta y$ and at $\Delta\Xi = \pm\Delta x$, $\Delta H = 0.25\Delta y$, where the shifting in y-direction had minor influence only. $\Delta\Xi = -\Delta x$ gives the desired downstream waves; $\Delta\Xi = +\Delta x$ gives upstream waves, $\Delta\Xi = 0$ waves in both directions.

For time-harmonic problems the SLE is complex. The real part of $\ln D$ is chosen as indicator of well-conditioning of the system. Results of numerical experiments for two grids ($n_x \cdot n_y = 41 \cdot 21$ and $41 \cdot 11$) are listed in Tab.7.1 for two parameter values $\alpha = \Delta y/\Delta x$. Both grids cover the same area. D_{opt} is the maximal value of D, obtained at $(\Delta\Xi/\Delta x)_{opt}$ and $(\Delta H/\Delta y)_{opt}$. D_0 is the value of D for $(\Delta\Xi/\Delta x)_{opt}$ and $\Delta H = 0$. The case $\tau = 0$ in Tab.7.1 corresponds to the steady case investigated by Jensen. A different optimum for the shift in y-direction is found. The reason lies in the lower height of the source layer above the free surface. Jensen's layer of sources is located $h_s = 2\Delta x$ above the collocation points, my layer of sources only $h_s = \Delta x$. However, the shift in y-direction is of minor importance and may even be excluded. Suitable shifting values seem to be independent of τ. Tab.7.2 demonstrates the neglible influence of h_s for $\tau = 1.0$ and $\alpha = 2$.

	$(\Delta\Xi/\Delta x)_{opt}$		$(\Delta H/\Delta y)_{opt}$		$\lvert D_0\rvert/\lvert D_{opt}\rvert$	
τ	$\alpha=1$	$\alpha=2$	$\alpha=1$	$\alpha=2$	$\alpha=1$	$\alpha=2$
0.0	0.95	1.01	0.03	0.02	0.798	0.939
0.5	0.95	1.01	0.03	0.02	0.780	0.934
1.0	0.95	1.00	0.03	0.02	0.782	0.929
1.5	0.94	1.00	0.03	0.02	0.773	0.925

Tab.7.1: Optimal values of shifting sources versus collocation points for 2 values of $\alpha = \Delta y/\Delta x$

$h_s/\Delta x$	$(\Delta\Xi/\Delta x)_{opt}$	$(\Delta H/\Delta y)_{opt}$
0.8	0.99	0.02
1.0	1.00	0.02
1.2	1.01	0.02

Tab.7.2: Influence of h_s on optimal shifting values ($\tau = 1.0$, $\alpha = 2$)

For $\tau = 1$ and depth of submergence $d = 0.45U^2/g$ *Nakos and Sclavounos (1990)* compared their RSM results with an analytical solution. The analytical solution does not appear to be very accurate outside of the sector of waves due to the particular integral representation of the solution used in the code (*Nakos*, personal communication). Figs.7.2 through 7.5 show that the shifting technique also gives very good agreement with the analytical solution in the wave sector for different τ-values. Compared are contour lines of the real (Figs.7.2, 7.3, 7.4) and the imaginary (Fig.7.5) part of the potential. The numerical solution was obtained with the following grid: $F_h = U/\sqrt{g\Delta x} = 0.6386$, $\alpha = 2$, $n_x = 65$, $n_y = 19$.

One method to validate RSM results is by checking how well the boundary condition is fulfilled between the collocation points. The most critical area is close to the submerged source. As an error criterion I use

$$\varepsilon = \frac{|-\omega^2\phi - 2i\omega U\phi_x + U^2\phi_{xx} - g\phi_z|}{\max(|\omega^2\phi|, |2i\omega U\phi_x|, |U^2\phi_{xx}|, |g\phi_z|)} \tag{80}$$

where ϕ is the total potential of submerged source and source layer above the free surface. For $\tau = 1.0$ with the above mentioned grid ($n_x = 65$, $n_y = 19$) the maximal error at a collocation point was $5 \cdot 10^{-5}$. At the point $(-\Delta x/2, 0, 0)$ the error was $1 \cdot 10^{-2}$ and at $(-\Delta x/2, \Delta y/2, 0)$ it was $8 \cdot 10^{-2}$. This can still be considered as reasonably good fulfillment of the boundary condition.

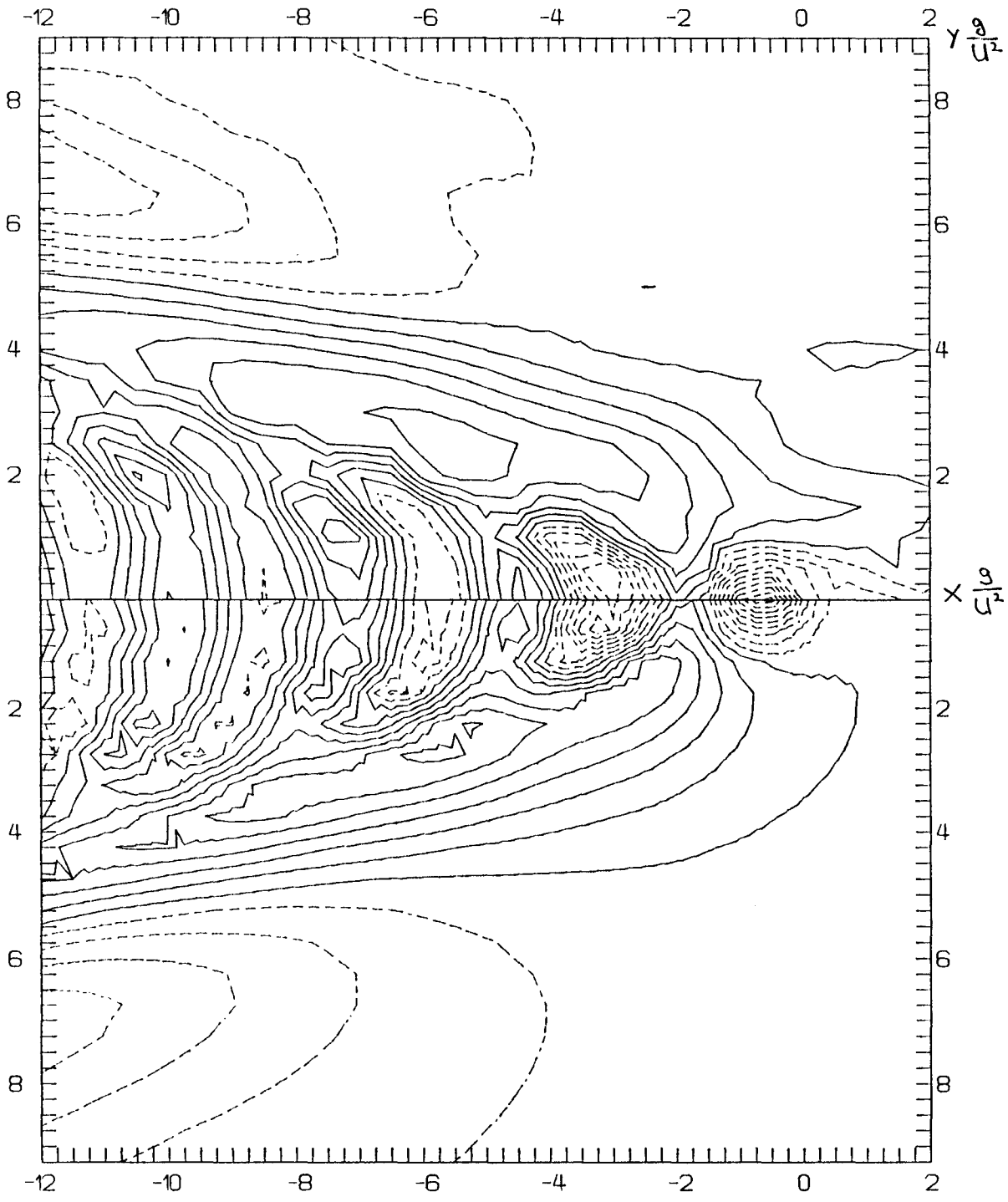

Fig.7.2: Contour lines of the real part of the velocity potential on the mean free surface due to a submerged time-harmonic source ($\tau = 0.8$), $U = 1\text{m/s}$, depth of submergence $d = 0.45U^2/g$. Comparison between the author's numerical solution (bottom-half) and the analytical solution of *Nakos* (top-half). Lines are spaced $\Delta\Phi = 0.2\text{m}^2/\text{s}$, dotted lines are positive values starting from $0.1\text{m}^2/\text{s}$, solid lines negative values starting from $-0.1\text{m}^2/\text{s}$.

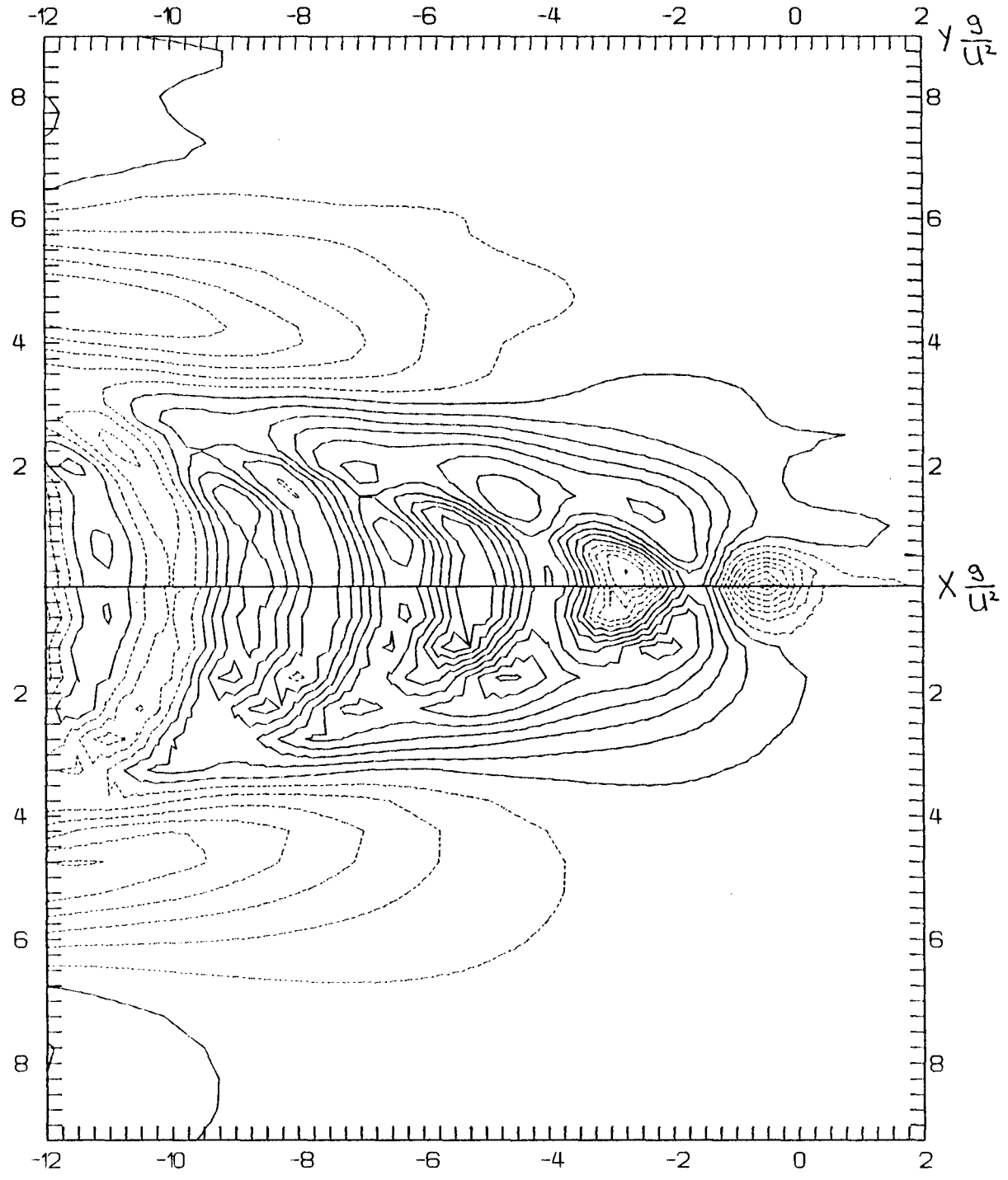

Fig.7.3: Contour lines of the real part of the velocity potential on the mean free surface due to a submerged time-harmonic source ($\tau = 1.0$), $U = 1\text{m/s}$, depth of submergence $d = 0.45U^2/g$. Comparison between the author's numerical solution (bottom-half) and the analytical solution of *Nakos* (top-half). Lines are spaced $\Delta\Phi = 0.2\text{m}^2/\text{s}$, dotted lines are positive values starting from $0.1\text{m}^2/\text{s}$, solid lines negative values starting from $-0.1\text{m}^2/\text{s}$.

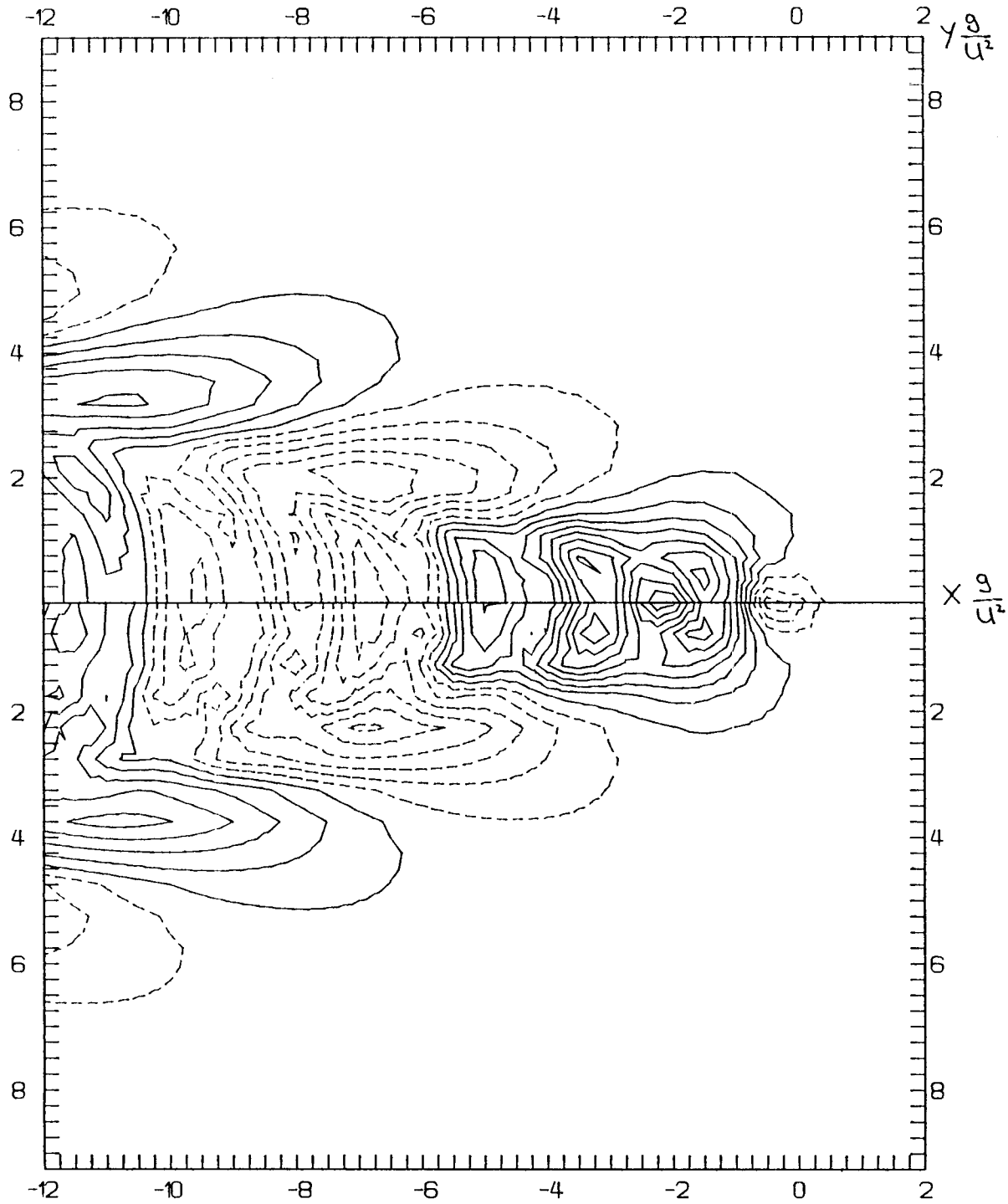

Fig.7.4: Contour lines of the real part of the velocity potential on the mean free surface due to a submerged time-harmonic source ($\tau = 1.5$), $U = 1\text{m/s}$, depth of submergence $d = 0.45U^2/g$. Comparison between the author's numerical solution (bottom-half) and the analytical solution of *Nakos* (top-half). Lines are spaced $\Delta\Phi = 0.2\text{m}^2/\text{s}$, dotted lines are positive values starting from $0.1\text{m}^2/\text{s}$, solid lines negative values starting from $-0.1\text{m}^2/\text{s}$.

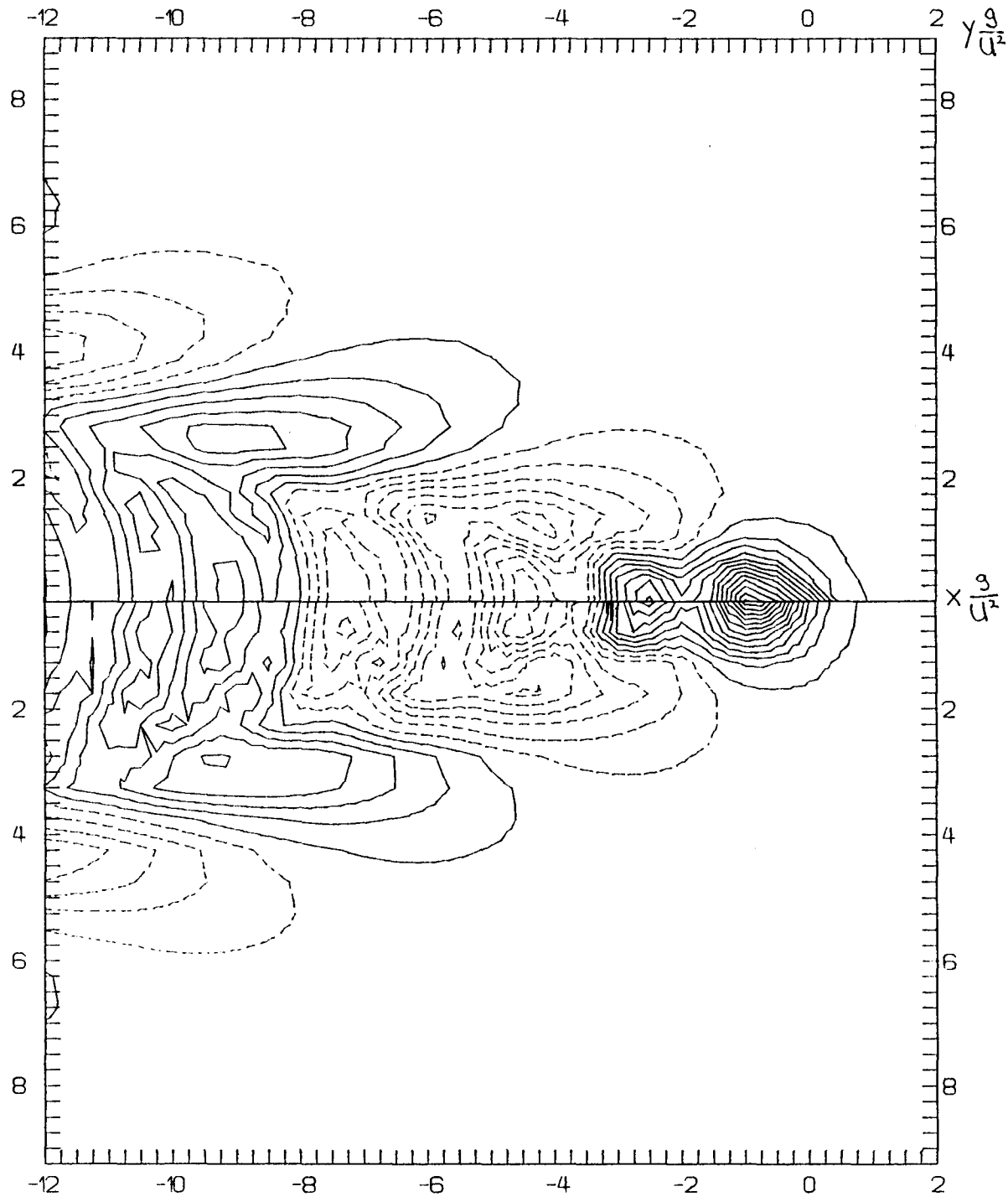

Fig.7.5: Contour lines of the imaginary part of the velocity potential on the mean free surface due to a submerged time-harmonic source ($\tau = 1.5$), $U = 1\text{m/s}$, depth of submergence $d = 0.45U^2/g$. comparison between the author's numerical solution (bottom-half) and the analytical solution of *Nakos* (top-half). Lines are spaced $\Delta\Phi = 0.2\text{m}^2/\text{s}$, dotted lines are positive values starting from $0.1\text{m}^2/\text{s}$, solid lines negative values starting from $-0.1\text{m}^2/\text{s}$.

8. Submerged Spheroid

8.1. Geometry

The submerged spheroid of Fig.8.1 ($L = 10$m, $D = 2$m) was chosen as a simple test case.

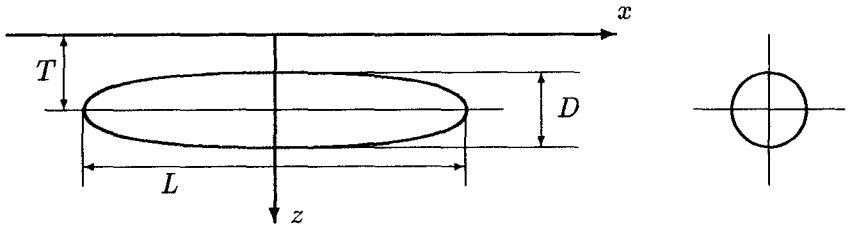

Fig.8.1: Submerged Spheroid $D/L = 0.2$

The total surface area of a spheroid is

$$S = \frac{1}{2}\pi LD\left(\frac{\arcsin\delta}{\delta} + \frac{D}{L}\right) \qquad \text{with} \quad \delta = \sqrt{1 - \frac{D^2}{L^2}} \tag{81}$$

For $D/L = 0.2$ this gives: $S = 2.5096LD$

The spheroid is discretized using panels of approximately same size. As symmetry in y-direction is exploited, numbers of panels should be understood as for one half of the body resp. as number of collocation points on the body. Figs.8.2 to 8.4 show different discretizations. Tab.8.1 shows the total surface area of the panels. The relative error of the surface area is a first indication of errors due to discretization.

	exact	20 panels	84 panels	172 panels	356 panels	1508 panels
S/LD	2.510	2.427	2.4835	2.4960	2.5025	2.5075
error		3.3%	1.0%	0.5%	0.3%	0.1%

Tab.8.1: Surface area of spheroid

8.2. Stationary problem

Beck and Doctors (1987) investigated the stationary flow extensively. The nonlinear problem was approximated by the Neumann-Kelvin problem. Beck and Doctors used Green functions that fulfilled automatically the linearized free-surface condition (19). They investigated convergence properties of their method for increasing panel numbers for $T/L = 0.16$ and $T/L = 0.245$ for a wide range of Froude numbers. For $T/L = 0.16$ *Sclavounos and Nakos (1988)* obtained good agreement with Beck and Doctors' lift and drag coefficients C_L and C_W using a Rankine source method with 400 panels on one half of the body.

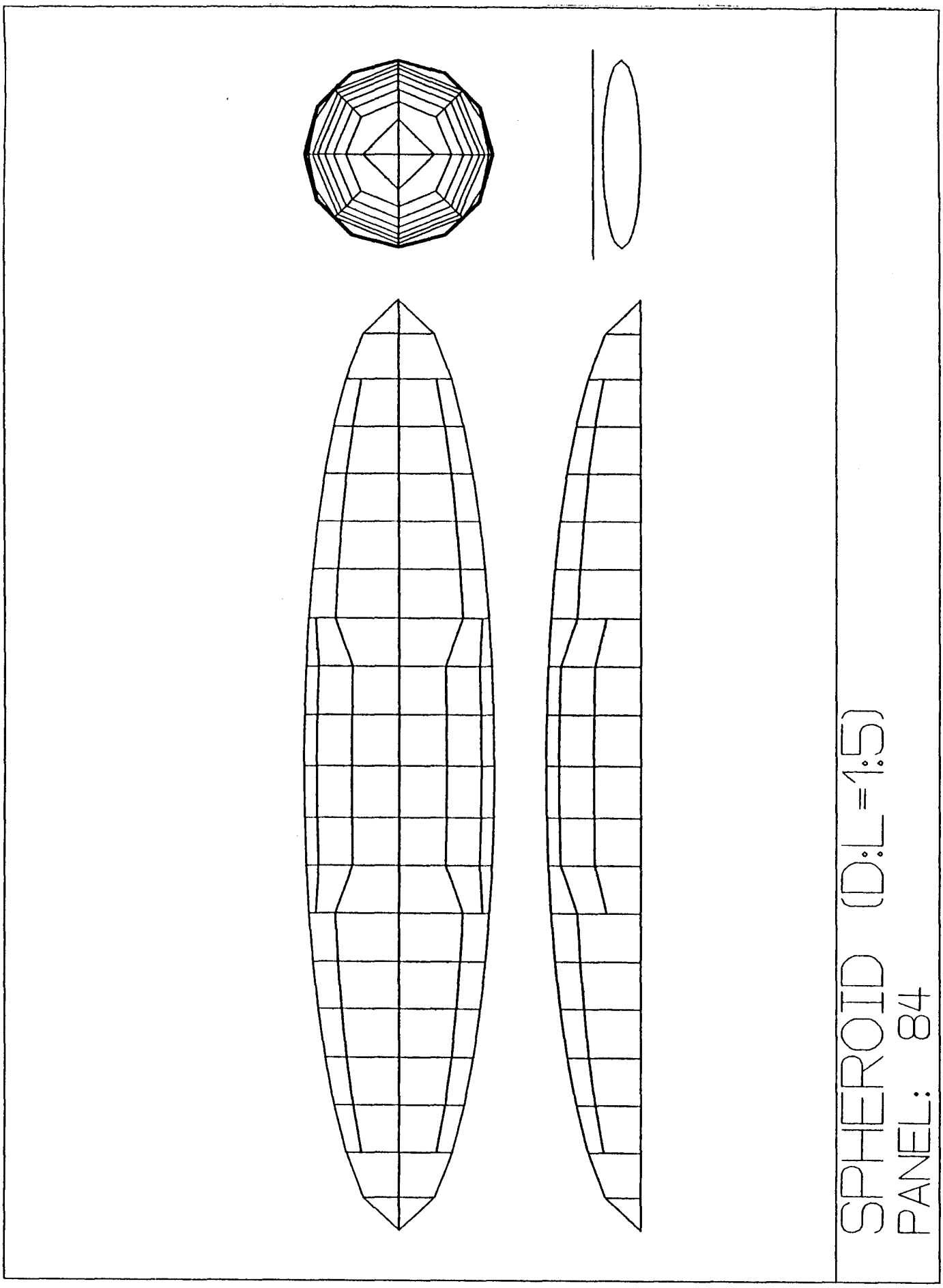

Fig.8.2: Hull discretization for spheroid (84 panels)

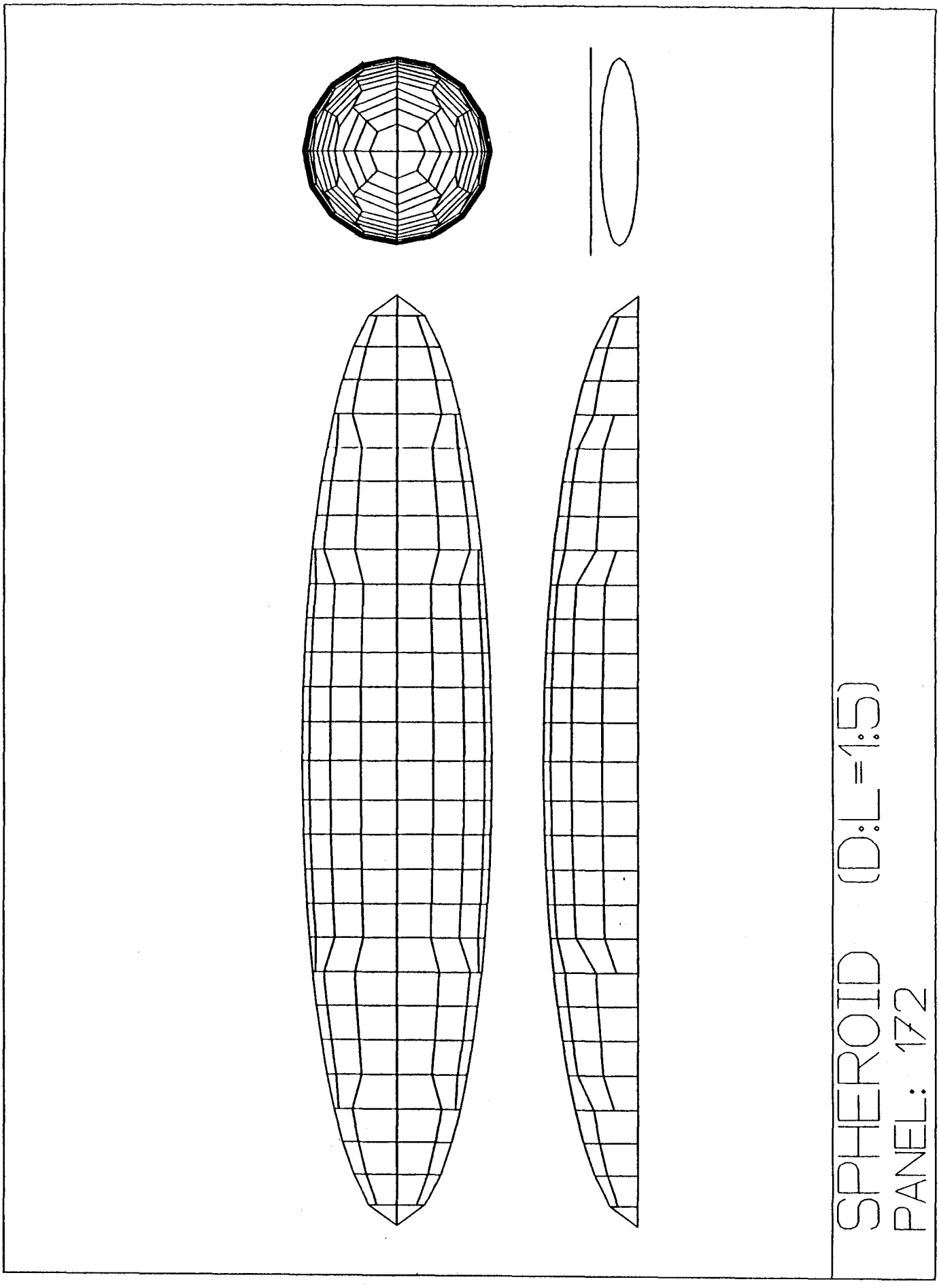

Fig.8.3: Hull discretization for spheroid (172 panels)

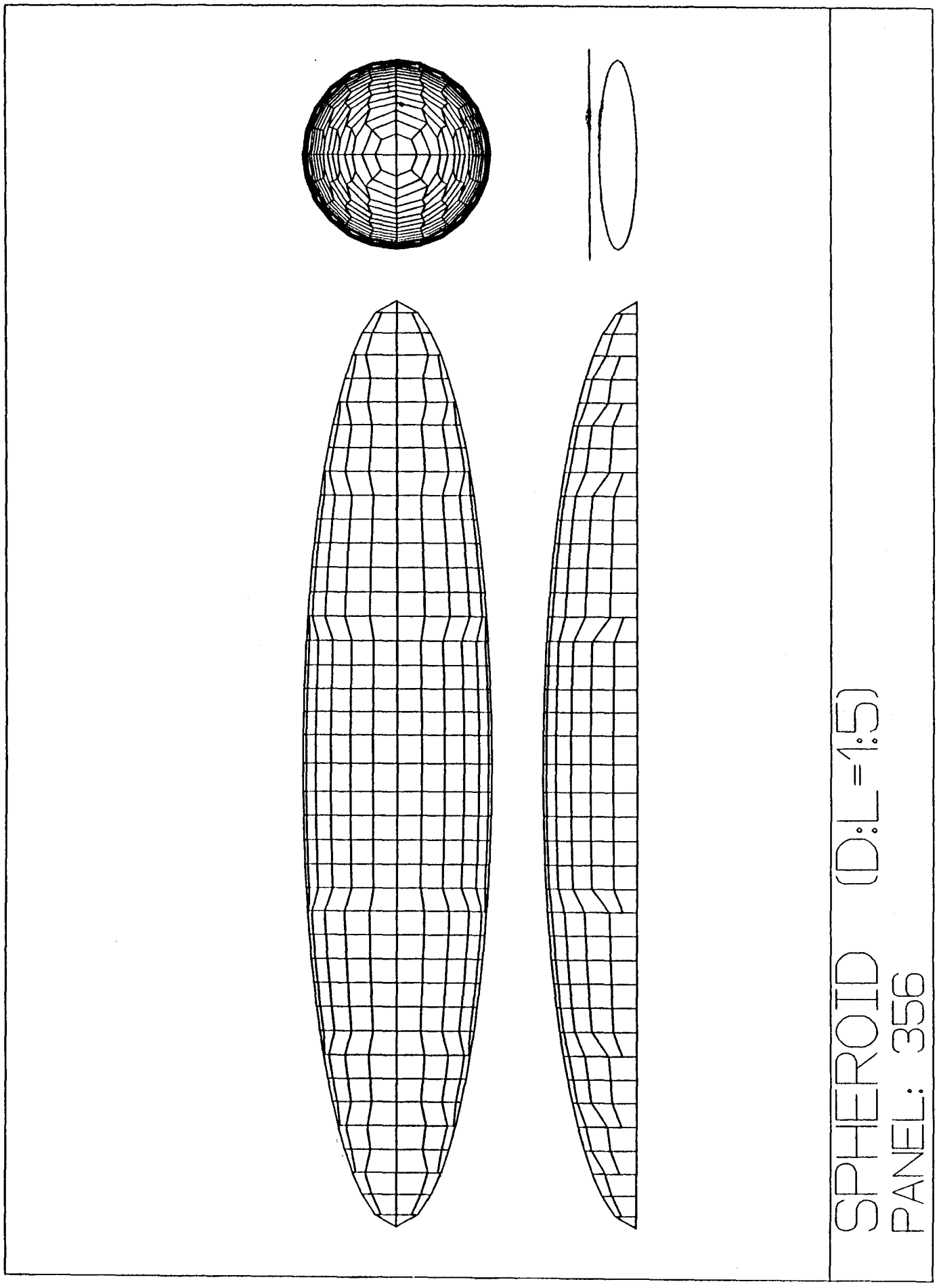

Fig.8.4: Hull discretization for spheroid (356 panels)

For different discretizations of the body I calculated Neumann-Kelvin lift, drag, and moment coefficients for $T/L = 0.16$:

$$C_W = -F_1^{nk}/\frac{1}{2}\rho U^2 S \tag{82}$$

$$C_L = -F_3^{nk}/\frac{1}{2}\rho U^2 S \tag{83}$$

$$C_M = M_2^{nk}/\frac{1}{2}\rho U^2 S L \tag{84}$$

where S is the total area of the panels.

The free-surface discretization was done automatically according to the following guidelines:

- grid spacing in x-direction: $\min(\lambda/8, 3 * \sqrt{\text{average body panel area}})$ with λ length of transverse waves
- grid spacing in y-direction: same as grid spacing in x-direction
- grid length before $x = 0$: λ
- grid length behind $x = 0$: max(0.6 ship length, λ)
- grid width: 1/3 of grid length
- height of source layer above collocation points: same as grid spacing in x-direction

For all Froude numbers good agreement with Beck and Doctors was found even for rather course discretizations of the body. Tab.8.2 to 8.4 give results. The solutions for 356 and 740 panels hardly differ indicating that body discretization errors become negligible here. For one discretization (356 panels), corresponding approximately to that of Nakos and Sclavounos, results are displayed in Fig.8.5.

F_n	20 panels	84 panels	356 panels	740 panels
0.26	0.00020	0.00013	0.00010	0.00010
0.28	0.00069	0.00068	0.00064	0.00063
0.30	0.00021	0.00020	0.00023	0.00023
0.32	0.00034	0.00027	0.00019	0.00018
0.34	0.00287	0.00219	0.00189	0.00185
0.40	0.0132	0.0133	0.0127	0.0128
0.50	0.0163	0.0180	0.0176	0.0175
0.60	0.0114	0.0127	0.0128	0.0127
0.70	0.00711	0.00819	0.00837	0.00832
0.80	0.00447	0.00545	0.00557	0.00553

Tab.8.2: Neumann-Kelvin results for C_W

F_n	20 panels	84 panels	356 panels	740 panels
0.26	0.00903	0.00972	0.00963	0.00960
0.28	0.0100	0.0106	0.0106	0.0105
0.30	0.0117	0.0122	0.0121	0.0120
0.32	0.0153	0.0158	0.0156	0.0155
0.34	0.0186	0.0202	0.0199	0.0198
0.40	0.0224	0.0231	0.0230	0.0232
0.50	0.00648	0.00832	0.0892	0.0896
0.60	-0.00202	-0.00134	-0.00076	-0.00074
0.70	-0.00516	-0.00513	-0.00466	-0.00463
0.80	-0.00615	-0.00631	-0.00607	-0.00606

Tab.8.3: Neumann-Kelvin results for C_L

F_n	20 panels	84 panels	356 panels	740 panels
0.26	-0.000113	-0.000099	-0.000085	-0.000086
0.28	-0.000078	-0.000048	-0.000035	-0.000042
0.30	0.000143	0.000251	0.000268	0.000258
0.32	-0.000486	-0.000451	-0.000341	-0.000340
0.34	-0.00274	-0.00249	-0.00227	-0.00226
0.40	-0.00920	-0.00984	-0.00958	-0.00966
0.50	-0.0108	-0.0119	-0.0117	-0.0117
0.60	-0.00826	-0.00902	-0.00902	-0.00900
0.70	-0.00589	-0.00659	-0.00661	-0.00660
0.80	-0.00428	-0.00500	-0.00501	-0.00501

Tab.8.4: Neumann-Kelvin results for C_M

For the 84-panel body at $F_n = 0.4$ the nonlinear solution was obtained using 4 iterative steps. The final solutions for C_W, C_L and C_M ($C_W = 0.0139$, $C_L = 0.0238$, $C_M = -0.0105$) showed little difference (4% for C_W, 3% for C_L, 6% for C_M) justifying the Neumann-Kelvin approach at least for low or medium Froude numbers for this case. For $F_n = 0.8$ partial surfacing of the body is predicted resulting in strong nonlinear effects especially for the lift coefficient.

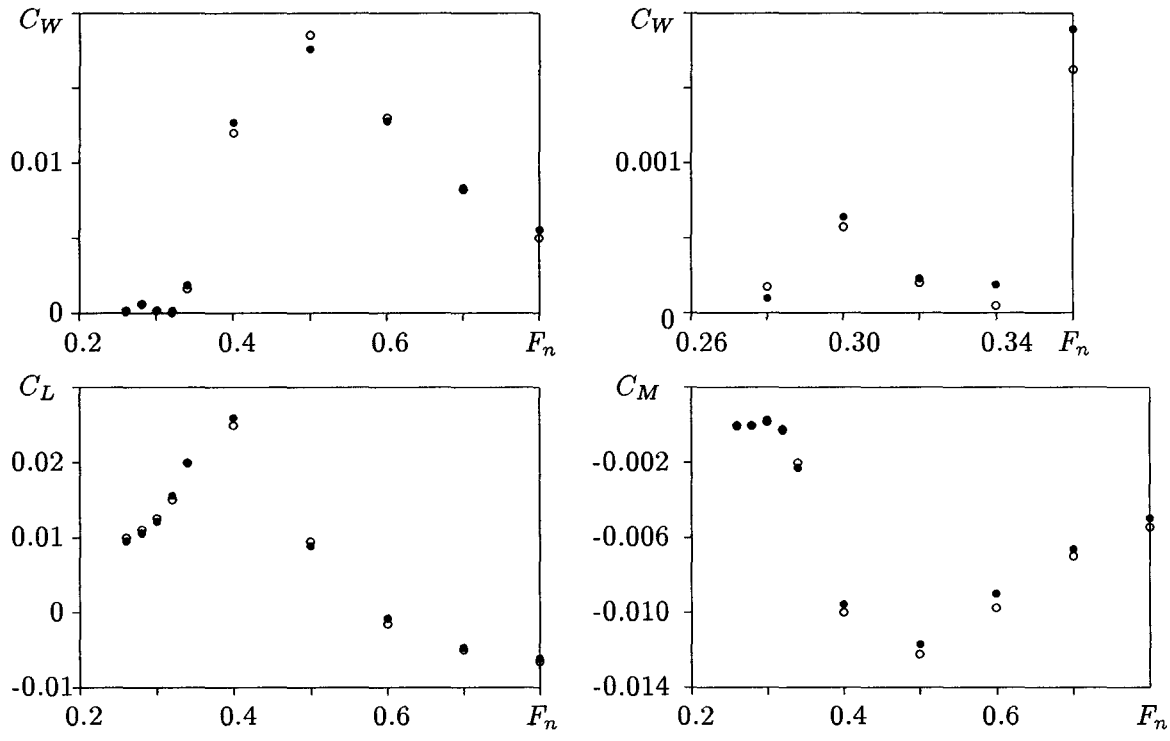

Fig. 8.5: C_W, C_L, C_M for submerged spheroid, Neumann-Kelvin solution
o Beck and Doctors, • Bertram (356 panels)

8.3. Diffraction problem

For $T/L = 0.15$ *Ohkusu and Iwashita (1989)* published computational and experimental results for $F_n = 0.2$ and head sea ($\mu = 180°$). Their computations were based on a Green function approach similar to that of Beck and Doctors for the steady problem. I investigated head and oblique sea according to Tab.8.5.

		$\mu = 180°$		$\mu = 150°$	
λ/L	$\omega[1/s]$	$\omega_e[1/s]$	τ	$\omega_e[1/s]$	τ
4.0	1.241	1.553	0.3135	1.511	0.3051
2.5	1.570	2.068	0.4176	2.001	0.4041
2.0	1.756	2.378	0.4802	2.294	0.4633
1.5	2.027	2.857	0.5769	2.746	0.5544
1.0	2.483	3.727	0.7527	3.561	0.7190
0.8	2.776	4.332	0.8747	4.123	0.8326
0.7	2.967	4.745	0.9582	4.507	0.9101
0.6	3.205	5.280	1.0660	5.002	1.0100
0.5	3.511	6.000	1.2120	5.667	1.1443
0.4	3.925	7.037	1.4210	6.620	1.3368

Tab.8.5: Incident waves for spheroid of $F_n = 0.2$

The non-zero parts of complex amplitudes of the Froude-Krilov forces (51) and moments (52) are:

$$Im(\hat{F}_1^{fk}) = -\rho g h \int_S -\sin(kx\cos\mu)\cos(ky\sin\mu)e^{-kz}n_1\,dS \tag{85}$$

$$Im(\hat{F}_2^{fk}) = -\rho g h \int_S \cos(kx\cos\mu)\sin(ky\sin\mu)e^{-kz}n_2\,dS \tag{86}$$

$$Re(\hat{F}_3^{fk}) = -\rho g h \int_S \cos(kx\cos\mu)\cos(ky\sin\mu)e^{-kz}n_3\,dS \tag{87}$$

$$Im(\hat{M}_1^{fk}) = -\rho g h \int_S \cos(kx\cos\mu)\sin(ky\sin\mu)e^{-kz}(yn_3 - zn_2)\,dS \tag{88}$$

$$Im(\hat{M}_2^{fk}) = -\rho g h \int_S -\sin(kx\cos\mu)\cos(ky\sin\mu)e^{-kz}(zn_1 - xn_3)\,dS \tag{89}$$

$$Re(\hat{M}_3^{fk}) = -\rho g h \int_S \sin(kx\cos\mu)\sin(ky\sin\mu)e^{-kz}(xn_2 - yn_1)\,dS \tag{90}$$

The inward unit normal of the spheroid is

$$\vec{n} = \left\{ \begin{array}{c} -x \\ -y(L/D)^2 \\ -z'(L/D)^2 \end{array} \right\} \frac{1}{\sqrt{x^2 + y^2(L/D)^4 + z'^2(L/D)^4}} \tag{91}$$

where $z' = z - T$ denotes the vertical component in a local coordinate system with origin in the center of the spheroid.

For numerical evaluation these integrals are transformed into double integrals exploiting symmetries, e.g. for $\mu = 180°$ and F_1^{fk}:

$$Im(\hat{F}_1^{fk}) = -4\rho g h \int_0^{L/2}\int_0^{\pi} \sin(kx)e^{-k(T+r\cos\alpha)}n_1\, r\sqrt{1 + (\partial r/\partial x)^2}\,d\alpha\,dx \tag{92}$$

$$r = \frac{D}{L}\sqrt{(L/2)^2 - x^2} \tag{93}$$

$$r\sqrt{1 + (\partial r/\partial x)^2} = \frac{D}{L}\sqrt{\frac{1}{4}L^2 - x^2\left(1 - \left(\frac{D}{L}\right)^2\right)} \tag{94}$$

In this form the integrals are evaluated numerically using the GINT-routine of *Söding (1979)*.

Table 8.6 compares results for Froude-Krilov forces and moments in head sea ($\mu = 180°$) obtained by strip method, direct integration (GINT) and panel integration for various discretizations and wave lengths λ. The relative error based on the GINT-results is small even for rather coarse discretizations. For results close to zero, naturally, the relative error increases. The error is inversely proportional to the number of panels. A 84-panel discretization is deemed to be sufficient to predict vertical Froude-Krilov force and moment about y-axis properly, but the horizontal force shows relative big errors. The strip method is based on a close-fit method for calculating sectional hydrodynamic coefficients, *Zhou (1988)*; 39 sections with 32 points each were used.

$1000Im(\hat{F}_1^{fk})/\rho ghLB$											
λ/L	GINT	84 panels		172 panels		356 panels		740 panels		strip method	
4.0	122.43	117.50	4.0%	120.38	1.7%	121.65	0.6%	122.14	0.2%	121.08	1.1%
2.5	154.60	148.73	3.8%	152.13	1.6%	153.64	0.6%	154.24	0.2%	152.38	1.2%
2.0	160.66	154.90	3.6%	158.21	1.5%	159.68	0.6%	160.28	0.2%	157.82	1.8%
1.5	149.19	144.60	3.1%	147.18	1.4%	148.34	0.6%	148.84	0.2%	145.38	2.6%
1.0	82.69	81.82	1.1%	82.17	0.6%	82.37	0.4%	82.52	0.2%	77.97	5.7%
0.8	30.39	31.54	3.8%	30.74	1.1%	30.43	0.1%	30.37	0.1%	26.38	13.2%
0.7	3.56	5.26	47.9%	4.19	17.6%	3.75	5.4%	3.61	1.4%	0.66	81.5%
0.6	-15.17	-13.70	9.7%	-14.56	4.1%	-14.91	1.7%	-15.06	0.7%	-16.29	7.4%
0.5	-16.01	-15.68	2.1%	-15.80	1.3%	-15.86	1.0%	-15.93	0.5%	-15.22	4.9%
0.4	-0.23	-0.81	247.8%	-0.43	84.8%	-0.29	23.9%	-0.25	6.5%	-0.80	247.8%
$1000Re(\hat{F}_3^{fk})/\rho ghLB$											
4.0	-122.43	-121.33	0.9%	-121.79	0.5%	-122.07	0.3%	-122.26	0.1%	-121.55	0.7%
2.5	-154.60	-153.26	0.9%	-153.86	0.5%	-154.21	0.3%	-154.42	0.1%	-153.49	0.7%
2.0	-160.66	-159.31	0.8%	-159.95	0.4%	-160.30	0.2%	-160.50	0.1%	-159.51	0.7%
1.5	-149.19	-148.05	0.8%	-148.69	0.3%	-148.99	0.1%	-149.12	0.05%	-148.13	0.7%
1.0	-82.69	-82.38	0.4%	-82.81	0.2%	-82.87	0.2%	-82.82	0.2%	-82.10	0.7%
0.8	-30.39	-30.63	0.8%	-30.87	1.6%	-30.74	1.1%	-30.58	0.6%	-29.87	1.7%
0.7	-3.56	-4.00	12.3%	-4.14	16.5%	-3.91	10.0%	-3.73	4.9%	-3.52	1.1%
0.6	15.18	14.71	3.1%	14.62	3.7%	14.92	1.7%	15.07	0.7%	15.07	0.7%
0.5	16.01	15.81	1.2%	15.71	1.9%	15.97	0.3%	16.03	0.06%	15.90	0.7%
0.4	0.23	0.27	13.0%	0.24	2.2%	0.32	34.8%	0.28	17.4%	-0.22	4.3%
$1000Im(\hat{M}_2^{fk})/\rho ghL^2B$											
4.0	9.39	9.28	1.2%	9.31	0.9%	9.33	0.6%	9.36	0.3%	9.70	3.3%
2.5	19.52	19.29	1.2%	19.34	0.9%	19.40	0.6%	19.45	0.4%	20.16	3.3%
2.0	26.06	25.76	1.2%	25.83	0.9%	25.91	0.6%	25.98	0.3%	26.92	3.3%
1.5	34.45	34.05	1.2%	34.16	0.8%	34.26	0.6%	34.35	0.3%	35.60	3.3%
1.0	36.96	36.56	1.1%	36.68	0.8%	36.81	0.4%	36.89	0.2%	38.24	3.5%
0.8	27.92	27.67	0.9%	27.76	0.6%	27.87	0.2%	27.91	0.03%	28.92	3.6%
0.7	18.86	18.75	0.6%	18.80	0.3%	18.88	0.1%	18.89	0.2%	19.56	3.7%
0.6	7.29	7.33	0.5%	7.34	0.7%	7.37	1.1%	7.34	0.7%	7.58	3.8%
0.5	-2.84	-2.72	4.2%	-2.72	4.2%	-2.75	3.2%	-2.80	1.4%	-2.95	3.9%
0.4	-3.87	-3.90	0.8%	-3.82	1.3%	-3.87	0.0%	-3.88	0.3%	-3.80	4.4%

Tab.8.6: Froude-Krilov forces and moments in head sea ($\mu = 180°$)
Results of direct numerical integration (GINT), panel and strip method
Moments about axes through body center
Relative error based on GINT-results

For oblique sea ($\mu = 150°$) panel results (172 panels) agree well both with direct integration and strip method results, Tab.8.7.

	$1000Im(\hat{F}_1^{fk})/\rho ghLB$			$1000Im(\hat{F}_2^{fk})/\rho ghLB$		
λ/L	GINT	172 panels	strip method	GINT	172 panels	strip method
4.0	107.63	105.82	106.51	62.14	61.98	61.71
2.5	139.27	137.01	137.47	80.41	80.21	79.87
2.0	148.20	145.86	145.92	85.56	85.35	84.99
1.5	145.48	143.36	142.43	83.99	83.80	83.45
1.0	99.44	98.43	95.39	57.41	57.33	57.08
0.8	54.81	54.65	50.87	31.64	31.64	31.48
0.7	27.32	27.58	23.92	15.77	15.81	15.70
0.6	1.48	2.00	0.78	0.85	0.91	0.84
0.5	-13.39	-12.95	-13.90	-7.73	-7.69	-7.72
0.4	-7.96	-7.95	-7.07	-4.59	-4.61	-4.60
	$1000Re(\hat{F}_3^{fk})/\rho ghLB$			$1000Im(\hat{M}_1^{fk})/\rho ghL^2B$		
4.0	-124.28	-123.62	-123.43	0	0	0
2.5	-160.82	-160.02	-159.73	0	0	0
2.0	-171.12	-170.32	-169.99	0	0	0
1.5	-167.98	-167.30	-166.90	0	0	0
1.0	-114.82	-114.68	-114.16	0	0	0
0.8	-63.29	-63.54	-62.97	0	0	0
0.7	-31.55	-32.00	-31.40	0	0	0
0.6	-1.71	-2.26	-1.69	0	0	0
0.5	15.46	14.99	15.44	0	0	0
0.4	9.19	9.03	9.19	0	0	0
	$1000Im(\hat{M}_2^{fk})/\rho ghL^2B$			$1000Re(\hat{M}_3^{fk})/\rho ghL^2B$		
4.0	8.22	8.15	8.49	-4.11	-4.09	-4.24
2.5	17.38	17.22	17.95	-8.69	-8.65	-8.97
2.0	23.58	23.37	24.35	-11.79	-11.74	-12.18
1.5	32.32	32.04	33.40	-16.16	-16.10	-16.70
1.0	39.01	38.70	40.34	-19.51	-19.44	-20.17
0.8	34.26	34.02	35.46	-17.13	-17.09	-17.73
0.7	27.50	27.34	28.48	-13.75	-13.72	-14.25
0.6	16.93	16.88	17.56	-8.46	-8.46	-8.78
0.5	4.15	4.22	4.32	-2.08	-2.10	-2.16
0.4	-3.94	-3.85	-4.10	1.97	1.96	2.05

Tab.8.7: Froude-Krilov forces and moments in oblique sea ($\mu = 150°$)
Results of direct numerical integration (GINT), panel and strip method
Moments about axes through body center
Relative error based on GINT-results

For head sea exciting forces were calculated using 84, 172 and 356 collocation points on the body. A rectangular grid symmetrical to $x = 0$ was used on the free surface. Within the area covered by the grid for the stationary computation, the surface elevation was linearly interpolated and derivatives of the stationary potential computed using the stationary panel distribution of known source strength. Outside this area, uniform flow and zero surface elevation was assumed.

λ/L	4.0	2.5	2.0	1.5	1.0	0.8	0.7	0.6	0.5	0.4
n_x	62	56	59	60	60	58	60	59	61	60
n_y	15	14	15	15	15	14	15	15	15	15
Δx	1.290	0.893	0.746	0.600	0.600	0.448	0.400	0.373	0.328	0.300

Tab.8.8: Variable grid parameters for surface grids

The grid parameters were adjusted to the wave length, using finer spacing for smaller λ. The nomenclature of chapter 7 is used. The following grid parameters were always the same: $\alpha = 2$, $h_s/\Delta x = 1$, $\Delta\Xi/\Delta x = 1.0$, $\Delta H/\Delta y = 0.02$. Tab.8.8 lists the variable grid parameters.

Tab.8.9 and Fig.8.6 compare RSM and strip-method results with experimental results of *Ohkusu and Iwashita (1989)*. Vertical forces agree well for a wide range of wave lengths with experiments and strip-method results. For the shortest wave length $\lambda/L = 0.4$, computational results differ drastically from experiments, probably due to experimental difficulties. Small changes in frequency result here in considerable changes in exciting forces. Both strip method and RSM overpredict the measured vertical force for wave lengths larger than $1.5L$. The reason lies possibly in neglecting viscous effects. Only for longer waves strip-method and RSM results for the force in x-direction and the moment about the y-axis differ noticably, mainly because the strip method does not account for the diffraction force in x-direction. The results for the 172-panel and 356-panel discretizations show little differences, indicating that errors due to the body discretization become negligible.

For $\mu = 150°$ exciting forces were calculated using 172 panels on the body. The same free-surface grids as for $\mu = 180°$ were used. Tab.8.10 and Fig.8.7 compare RSM and strip-method results. The agreement is similar as for $\mu = 180°$.

	$1000\,\lvert\hat{F}_1^e\rvert/\rho g h L B$				$1000\,\lvert\hat{F}_3^e\rvert/\rho g h L B$				$1000\,\lvert\hat{M}_2^e\rvert/\rho g h L^2 B$			
λ/L	strip	84	172	356	strip	84	172	356	strip	84	172	356
4.0	121	147	153	154	345	322	309	307	4.7	14.2	14.9	14.7
2.5	152	180	183	184	449	423	404	400	27.4	37.8	36.2	35.6
2.0	157	182	185	186	466	433	413	408	49.1	55.7	53.9	53.2
1.5	145	160	161	162	385	379	361	358	73.6	81.6	78.1	76.9
1.0	78	72	71	71	192	170	163	162	80.7	85.9	82.9	82.0
0.8	26	18	17	17	78	66	60	59	55.6	61.1	58.5	58.2
0.7	1	11	13	13	63	59	58	56	32.8	38.8	36.8	36.8
0.6	16	21	23	23	66	70	68	68	11.6	14.4	13.1	13.3
0.5	15	16	17	17	44	49	46	46	15.5	13.2	13.1	12.7
0.4	1	1	2	2	9	7	5	5	10.0	11.3	11.0	11.0

Tab.8.9: Exciting forces and moments in head sea ($\mu = 180°$), $F_n = 0.2$
results of RSM and strip method
moments about axes through body center

	$\frac{1000\lvert\hat{F}_1^e\rvert}{\rho g h L B}$		$\frac{1000\lvert\hat{F}_2^e\rvert}{\rho g h L B}$		$\frac{1000\lvert\hat{F}_3^e\rvert}{\rho g h L B}$		$\frac{1000\lvert\hat{M}_2^e\rvert}{\rho g h L^2 B}$		$\frac{1000\lvert\hat{M}_3^e\rvert}{\rho g h L^2 B}$	
λ/L	strip	172	strip	172	strip	172	strip	172	strip	172
4.0	107	140	169	151	342	306	7.5	14.1	3.4	2.8
2.5	138	168	226	195	454	415	19.7	30.1	9.7	11.4
2.0	146	174	241	206	481	435	39.3	45.9	19.2	19.7
1.5	143	161	225	197	422	406	64.5	70.0	32.9	32.0
1.0	95	91	139	128	257	234	82.9	85.2	44.7	42.5
0.8	51	39	73	69	115	108	69.0	70.9	39.4	38.2
0.7	24	13	35	38	61	54	50.8	53.9	30.7	31.3
0.6	1	10	23	23	52	47	26.9	30.4	18.4	20.0
0.5	14	16	27	27	59	55	7.9	6.8	4.4	6.5
0.4	7	7	12	16	20	23	13.6	11.2	6.5	5.2

Tab.8.10: Exciting forces and moments in oblique sea ($\mu = 150°$)
results of RSM and strip method
moments about axes through body center

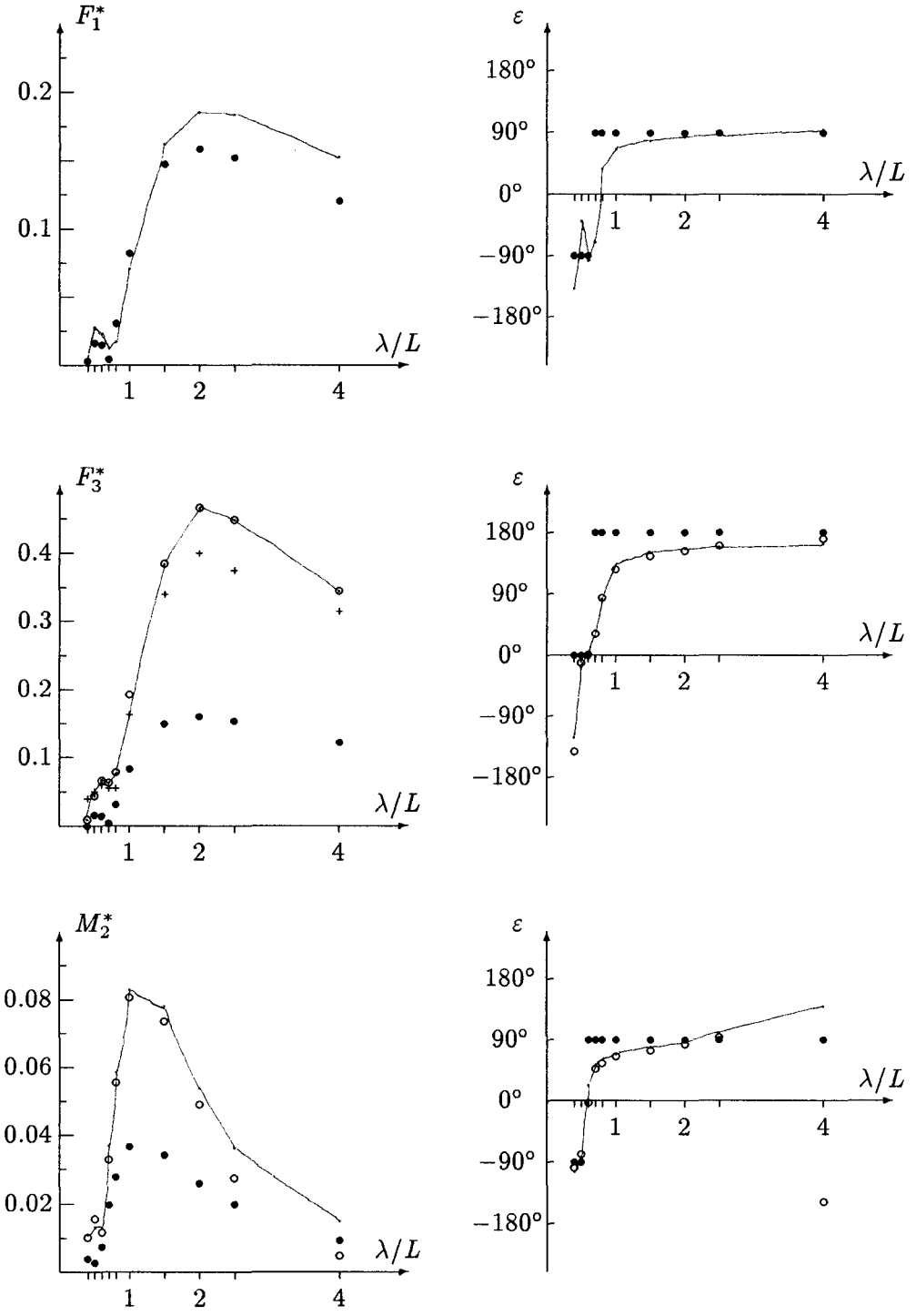

Fig.8.6: Exciting forces for spheroid (D:L=0.2) in head seas at $F_n = 0.2$, comparison of experiments (+), strip method (o) and panel method (—); Froude-Krilov (•)
$F_1^* = |\hat{F}_1^e|/\rho ghLB$, $F_3^* = |\hat{F}_3^e|/\rho ghLB$, $M_2^* = |\hat{M}_2^e|/\rho ghL^2B$
moment about axis through body center

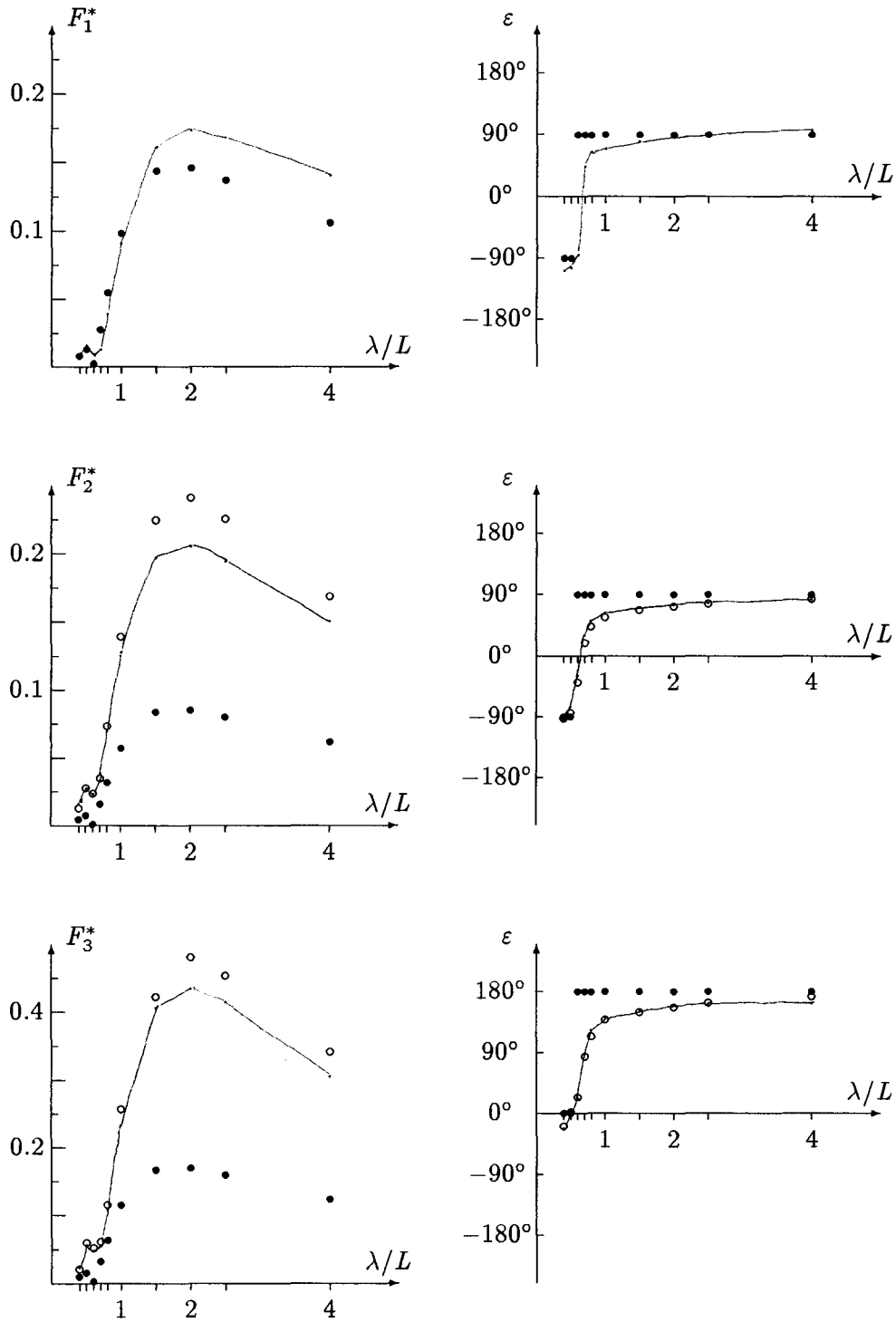

Fig.8.7a: Exciting forces for spheroid (D:L=0.2) in oblique sea ($\mu = 150°$) at $F_n = 0.2$; comparison of strip method (○) and panel method (—); Froude-Krilov (•)
$F_1^* = |\hat{F}_1^e|/\rho ghLB$, $F_2^* = |\hat{F}_2^e|/\rho ghLB$, $F_3^* = |\hat{F}_3^e|/\rho ghLB$

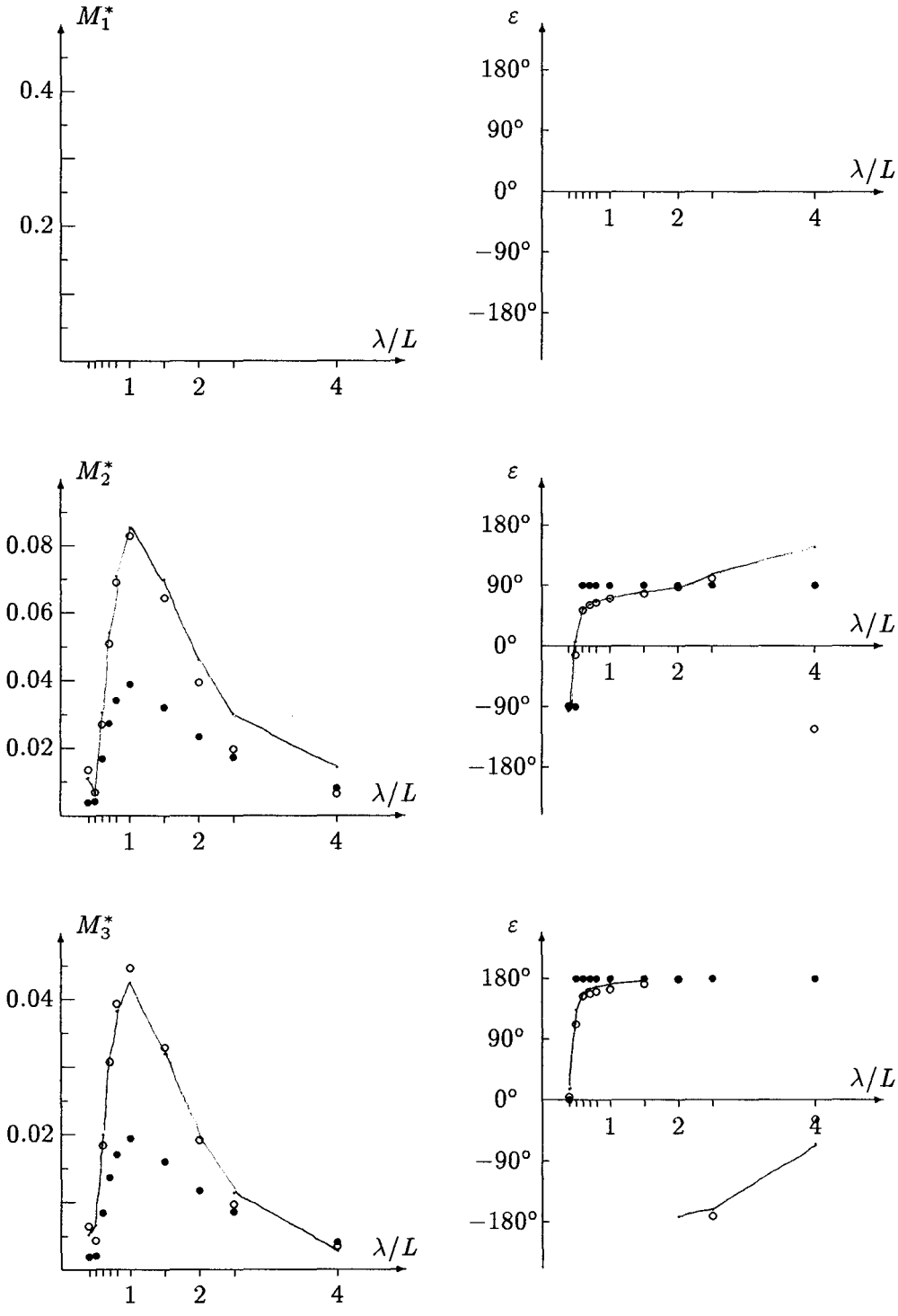

Fig.8.7b: Exciting moments for spheroid (D:L=0.2) in oblique sea ($\mu = 150°$) at $F_n = 0.2$; comparison of strip method (o) and panel method (—); Froude-Krilov (•)
$M_1^* = |\hat{M}_1^e|/\rho g h L^2 B$, $M_2^* = |\hat{M}_2^e|/\rho g h L^2 B$, $M_3^* = |\hat{M}_3^e|/\rho g h L^2 B$
moments about axes through body center

9. Series 60 ($C_B = 0.7$)

9.1 Geometry

The Series 60 parent hull form with $C_B = 0.7$, *Todd (1963)* model 4212, was chosen as a more realistic test case for validation. Tab.9.1 lists the principal ship characteristics.

L	B	T	C_B
121.92 m	17.42 m	6.97 m	0.7

Tab.9.1: Principal characteristics of Series 60 parent form ($C_B = 0.7$)

Fig.9.1 and 9.2 show control lines for a mathematical description of the ship's surface using EUMEDES, *Söding and Gerlach (1987)*, *Söding and Tonguc (1989)*.

9.1 Stationary problem

The stationary problem was solved using *Jensen's (1988)* method. The free-surface condition is met iteratively. Trim and sinkage are corrected in each iteration step so that forces and moments are in equilibrium. Moments include the effect of viscous and wave resistance, towing force, buoyancy and weight. *Jensen (1988)* recommends for calculations of trim the inclusion of an estimated frictional moment.

The hull surface was panelized up to a height of $0.25T$ above the still water line. 342 triangular and quadrilateral panels were used on one half of the ship, Fig.9.3. The origin of the coordinate system is at midship section, plane of symmetry in the still water line. The horizontal towing force was applied at the origin. The viscous resistance coefficient C_F was estimated to be $C_F = 0.003$ for all speeds. It was assumed that the center of gravity lies in the still water line.

The free-surface grids were created automatically for each Froude number. A rectangular grid is transformed following with its innermost line in a distance $\Delta x/2$ the still-water line. Some points located in the forward outer area of the rectangle – where no considerable disturbance of the uniform flow and thus no waves are expected – are eliminated to reduce the number of collocation points and thus computational time. Fig.9.4 shows a typical grid created this way. The nomenclature of chapter 7 is used. x_1 denotes the foremost x-value, $n < n_x \cdot n_y$ the number of points in the free-surface grid. The following grid parameters were always the same: $\alpha = 2$, $h_s/\Delta x = 1$. Shifting of collocation points versus source points is done by adding in each longitudinal line one collocation point at the upstream end and one source point at the downstream end, Fig.9.4. Tab.9.2 lists the variable grid parameters.

F_n	n_x	n_y	n	x_1	Δx [m]
0.20	71	23	847	100	3.3
0.25	50	16	508	110	5
0.30	50	16	510	130	7

Tab.9.2: Variable grid parameters for free-surface grids

Todd (1963) gives experimental values for the total resistance coefficient C_T. The model results ($L = 20$ ft) were converted to apply to ships of $L = 400$ ft $= 121.92$ m. In making this conversion, the ATTC 1947 friction formulation was used together with an addition of 0.0004 for model-ship correlation allowance C_A.

Fig.9.1: EUMEDES control lines for Series 60 $C_B = 0.7$; front view

Fig.9.2: EUMEDES control lines for Series 60 $C_B = 0.7$; perspective view

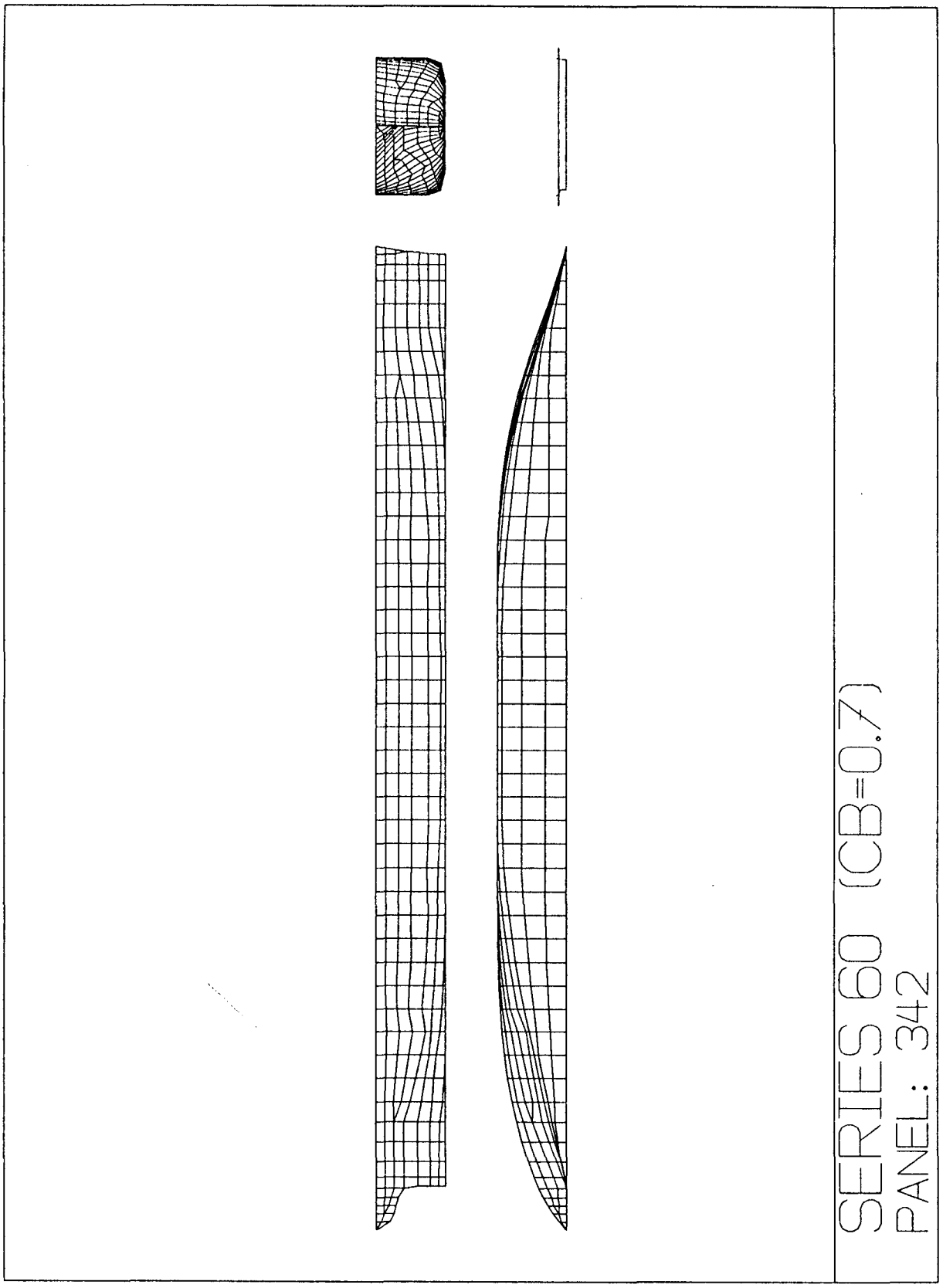

Fig.9.3: Hull discretization for Series 60 $C_B = 0.7$

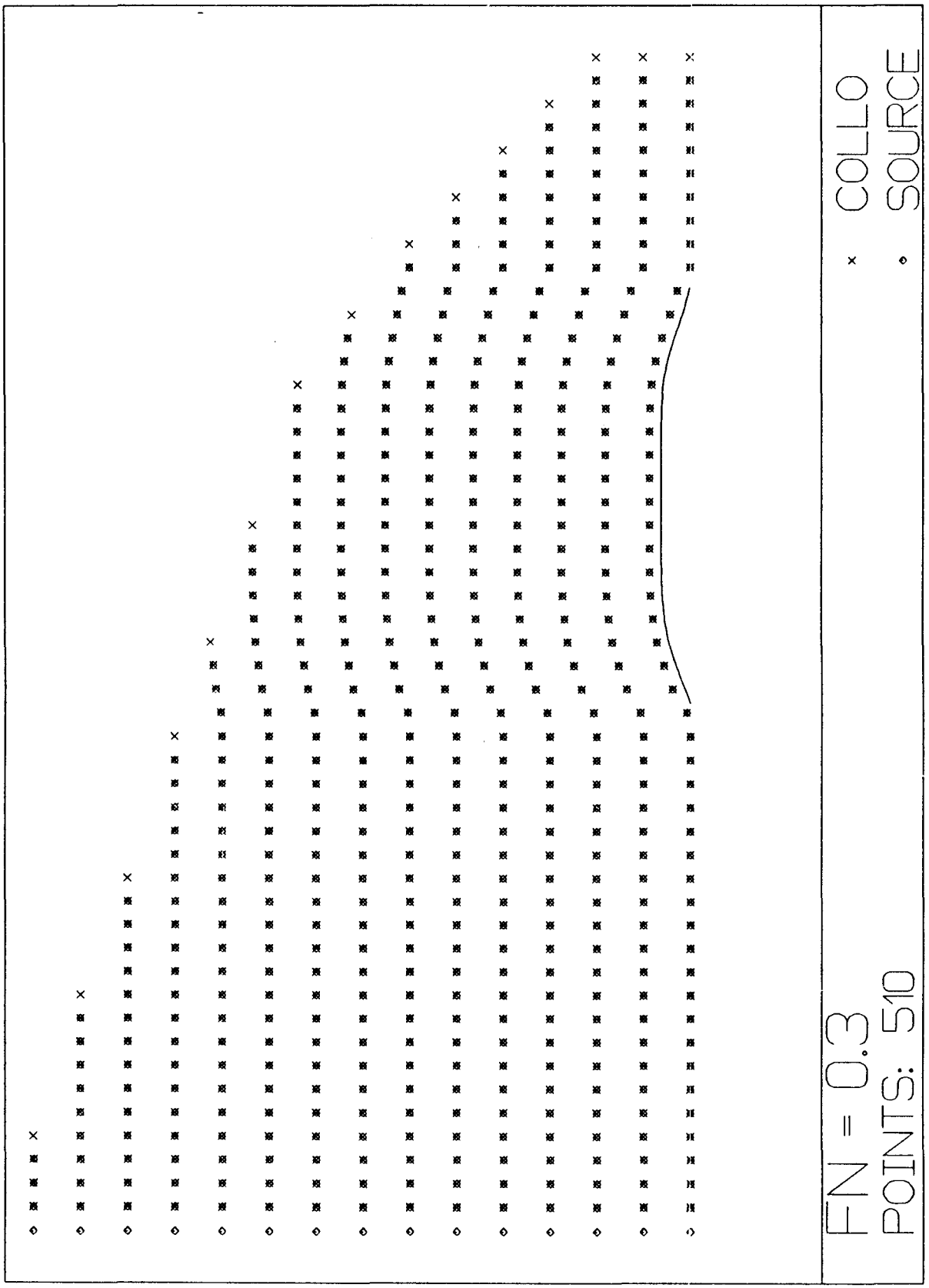

Fig.9.4: Typical free-surface discretization for Series 60 $C_B = 0.7$

Reconstruction of the model values (index m) from the ship values (index s) follows from

$$C_{Tm} = C_{Ts} - (C_{Fs} + 0.0004) + C_{Fm} \tag{95}$$

with C_F according to ATTC:

$$C_F = \left(\frac{0.242}{\log(R_n C_F)}\right)^2 \tag{96}$$

$R_n = UL/\nu$. The kinematic viscosity ν was assumed to be $10^{-6}\mathrm{m}^2/\mathrm{s}$.

Using a form factor 0.09 – based on the ITTC 1978 prediction method for single-screw ships, *Harvald (1983)* – the wave resistance coefficient is estimated to

$$C_W = C_{Tm} - C_{Fm}(1 + 0.09) \tag{97}$$

with C_F according to ITTC:

$$C_F = \frac{0.075}{(\log R_n - 2)^2} \tag{98}$$

Tab.9.3 lists the C_W-values determined this way. The first two columns are Todd's published data.

$\frac{U}{\sqrt{L_{WL}}}\ [\frac{\mathrm{kn}}{\sqrt{\mathrm{ft}}}]$	$C_{Ts} \cdot 10^3$	F_n	$C_W \cdot 10^3$
0.60	2.866	0.164	0.447
0.65	2.915	0.178	0.536
0.70	2.956	0.200	0.627
0.75	3.155	0.216	0.763
0.80	3.445	0.231	1.054
0.85	3.711	0.253	1.479
0.90	4.652	0.268	2.435
0.95	6.602	0.283	4.399
1.00	8.662	0.297	6.473
1.05	9.918	0.312	7.741
1.10	10.049	0.327	7.884
1.15	9.596	0.342	7.442
1.20	9.323	0.357	7.180

Tab.9.3: C_W for Series 60 ($C_B = 0.7$) from Todd's experiments

Computations were performed on a VAX 6310. For 342 collocation points on the body and 510 on the free surface, 86 CPU minutes were used for 4 iteration steps. Fig.9.5 compares the non-linear computational results (4. iteration step) with Todd's experimental values. For all 3 Froude numbers agreement is satisfactory.

In each iteration step an error in fulfilling the non-linear free-surface condition is evaluated:

$$\text{error} = \max \frac{\left|\frac{1}{2}\nabla\phi_i \nabla(\nabla\phi_i)^2 - g\frac{\partial\phi_i}{\partial z}\right|}{gU} \tag{99}$$

where ϕ_i is the potential at collocation point i, and the maximum is taken over all points i on the free surface. Tab.9.4 lists C_W results and corresponding errors. The error decreases by two orders of magnitude in 4 iterations.

	step 1		step 4	
F_n	C_W	error	C_W	error
0.20	0.00110	0.0666	0.00083	0.000968
0.25	0.00204	0.0682	0.00160	0.000759
0.30	0.00551	0.0465	0.00589	0.000334

Tab.9.4: C_W and free-surface error for first and last iteration step

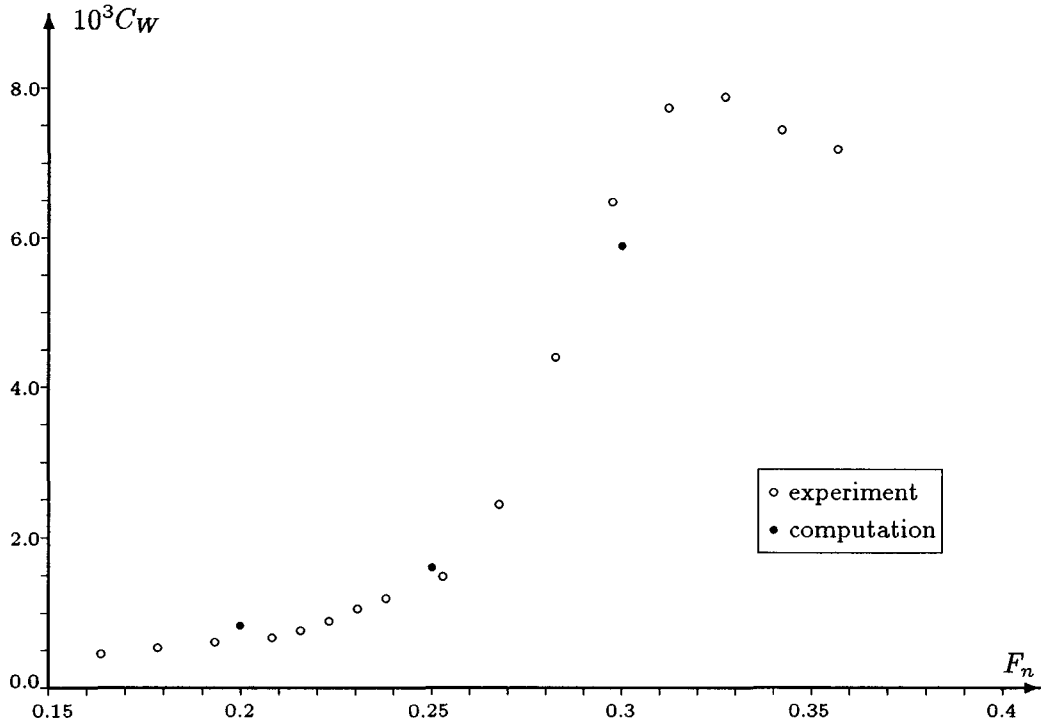

Fig.9.5: Wave resistance coefficient for Series-60 ($C_B = 0.7$); comparison of experiments (Todd) and computations

Figs.9.6 to 9.8 show the computed wave patterns for the 3 Froude numbers considered. The patterns seem plausible. The over-prediction of wave heights in the stern region – waves are higher than at the bow – is a typical phenomenon in potential flow calculations, compare e.g. *Jensen (1988)* for a Series 60 parent form ($C_B = 0.6$).

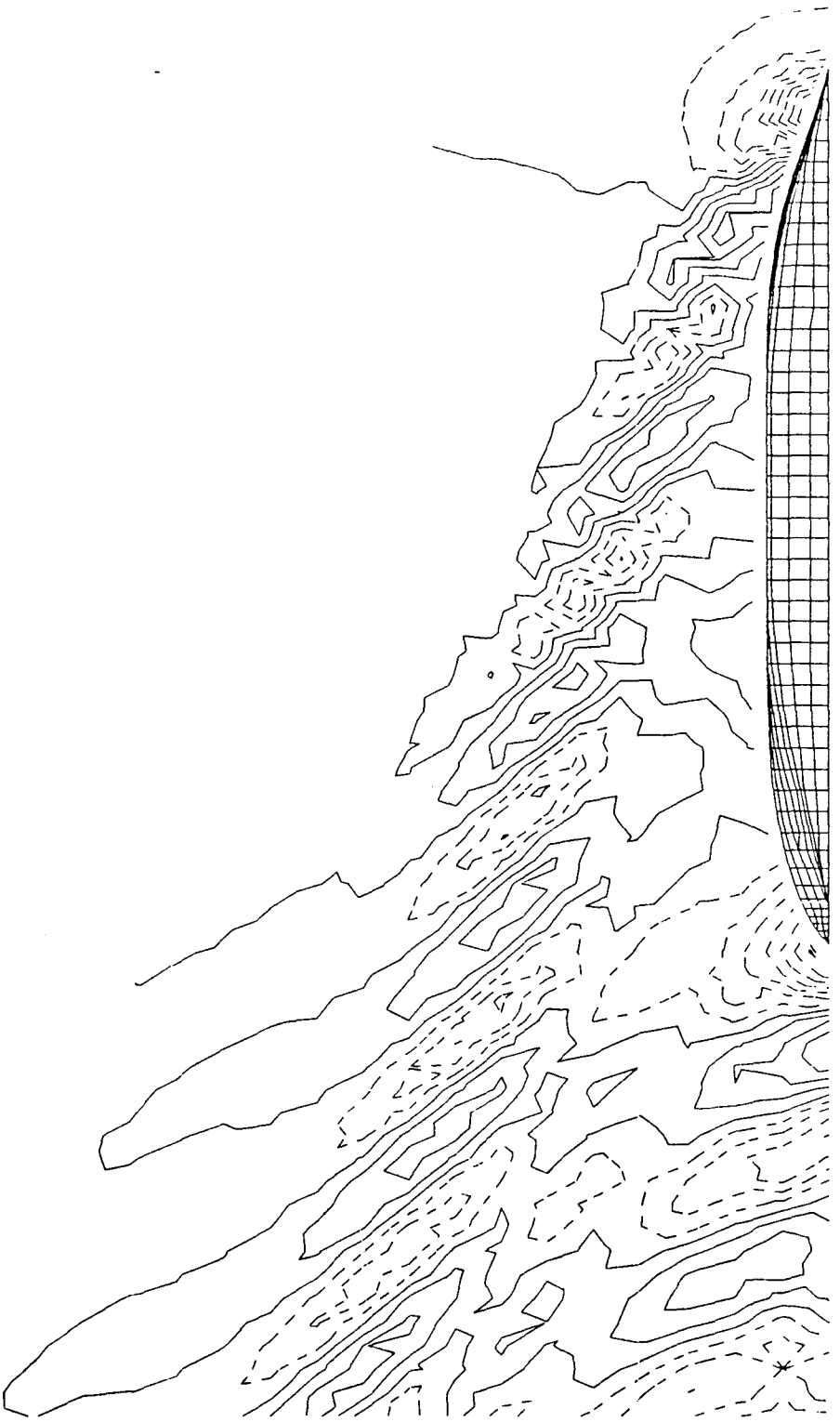

Fig.9.6: Contour lines of deformed water surface for Series 60 $C_B = 0.7$ at $F_n = 0.2$
vertical distance between contour lines $10^{-3}L$
dotted lines wave crests, solid lines troughs

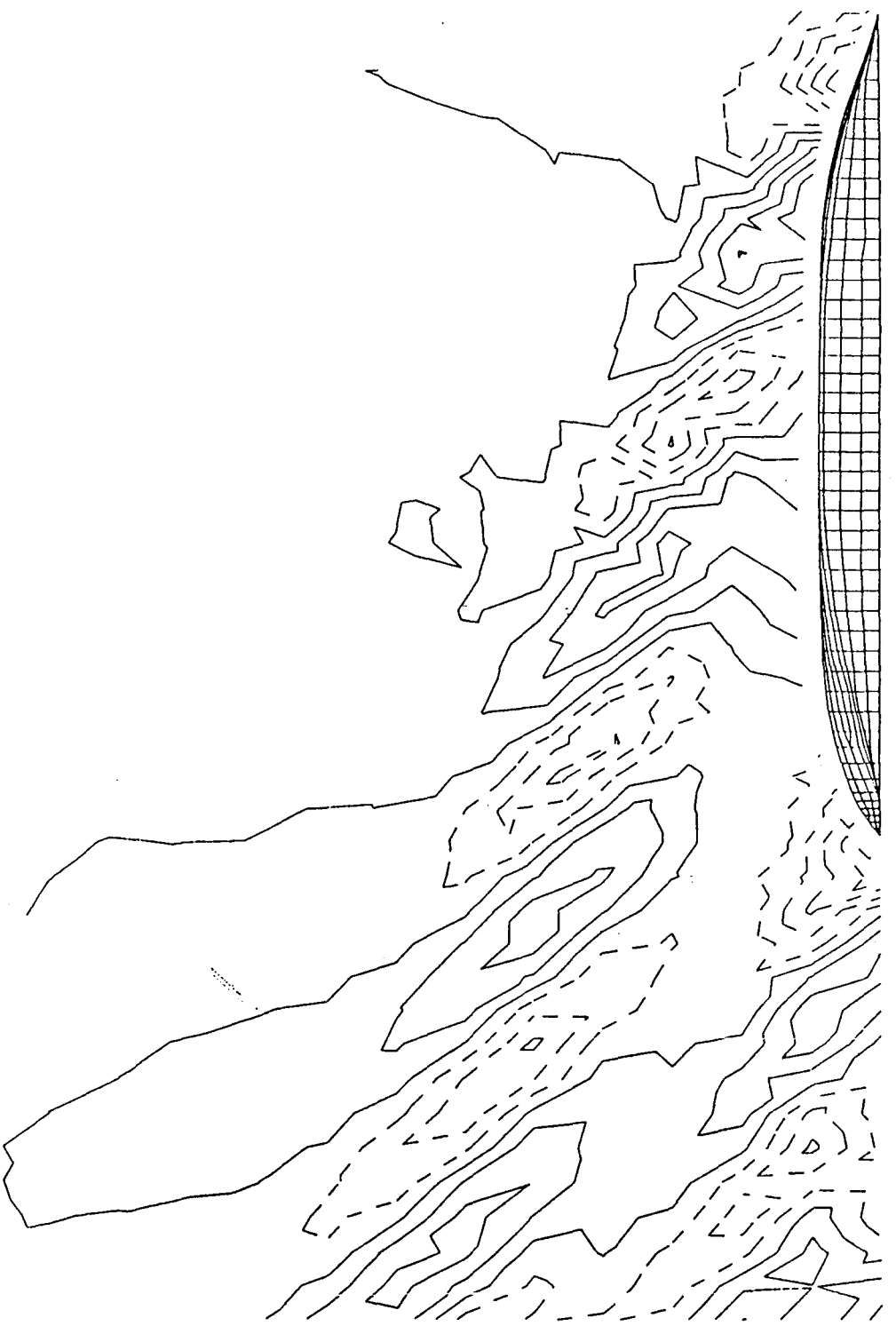

Fig.9.7: Contour lines of deformed water surface for Series 60 $C_B = 0.7$ at $F_n = 0.25$
vertical distance between contour lines $2 \cdot 10^{-3} L$
dotted lines wave crests, solid lines troughs

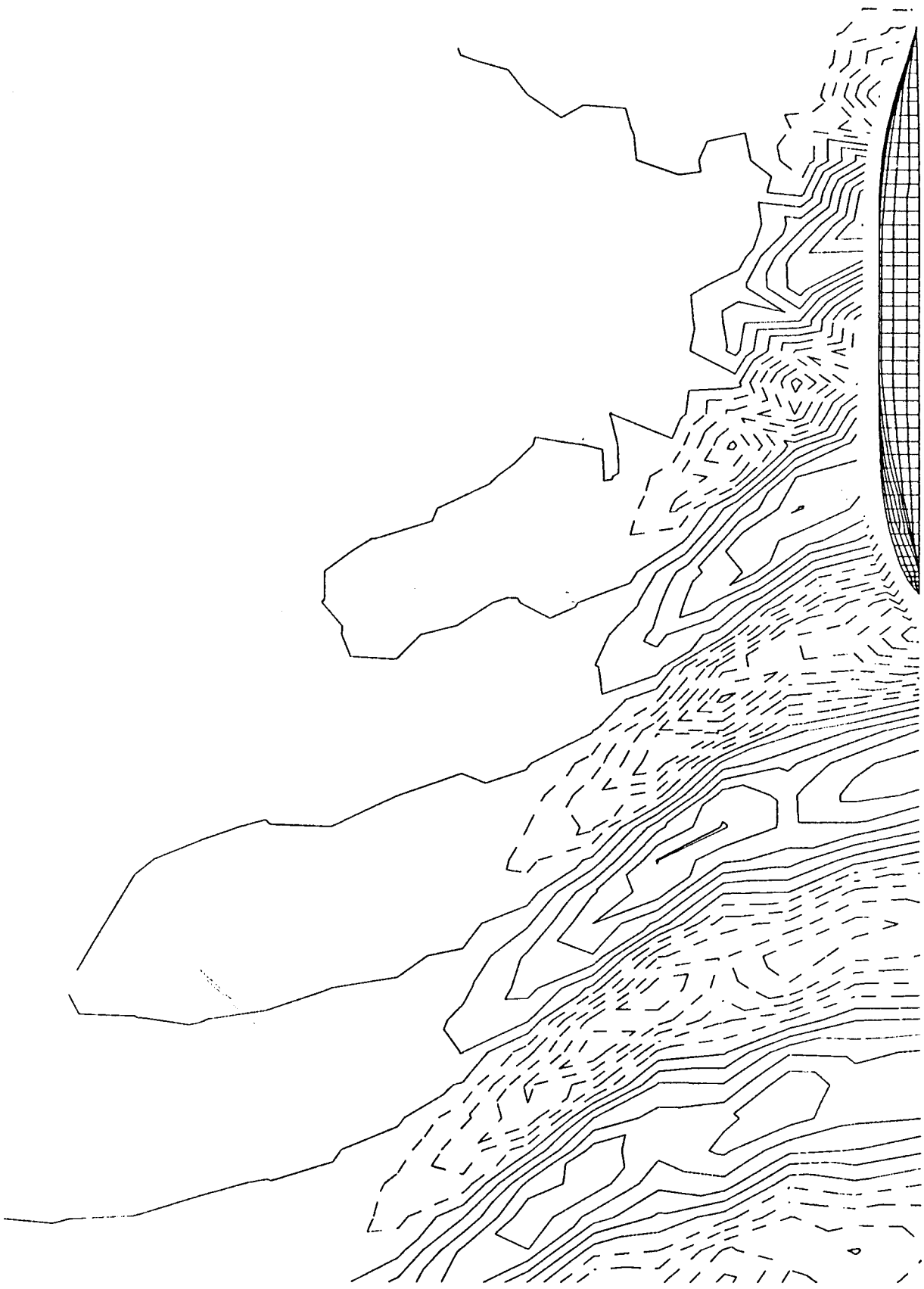

Fig.9.8: Contour lines of deformed water surface for Series 60 $C_B = 0.7$ at $F_n = 0.3$
vertical distance between contour lines $2 \cdot 10^{-3} L$
dotted lines wave crests, solid lines troughs

9.3. Diffraction problem

Gerritsma (1960) and *Gerritsma and Beukelman (1967)* experimentally investigated the seakeeping characteristics for various Froude numbers. All experiments were for head sea only and $\tau > 0.25$. The service speed of ship corresponds to $F_n = 0.208$, *Todd (1953)*. Later computations focussed on $F_n = 0.2$ being the Froude number closest to the service speed with experimental data available. *Beck and Magee (1988)* give a compendium of computational and experimental results for exciting forces in head sea. Tab.9.5 lists authors, methods, Froude numbers and force and moment components of published data which I use for comparison.

reference	method	F_n	1	3	5
Sclavounos (1984)	unified theory	0.2		+	+
Beck and Magee (1988)	time domain	0.2	+	+	+
	strip theory	0.2	+	+	+
Gerritsma (1960)	experiment	0.15,0.2,0.25,0.3		+	+
Gerritsma and Beukelman (1967)	experiment	0.15,0.3		+	+

Tab.9.5: References for the diffraction problem in head sea for Series 60 $C_B = 0.7$

I investigated head and oblique sea according to Tab.9.6.

		$F_n = 0.2$, $\mu = 180°$		$F_n = 0.25$, $\mu = 180°$		$F_n = 0.3$, $\mu = 180°$		$F_n = 0.2$, $\mu = 150°$	
λ/L	$\omega[1/s]$	$\omega_e[1/s]$	τ	$\omega_e[1/s]$	τ	$\omega_e[1/s]$	τ	$\omega_e[1/s]$	τ
0.50	1.006	1.718	1.212	1.897	1.672	2.075	2.194	1.623	1.144
0.75	0.821	1.296	0.914	1.415	1.247	1.534	1.622	1.233	0.869
1.00	0.711	1.067	0.753	1.157	1.019	1.246	1.317	1.020	0.719
1.25	0.636	0.921	0.649	0.992	0.875	1.064	1.125	0.883	0.623
1.50	0.581	0.818	0.577	0.878	0.773	0.937	0.991	0.786	0.554
1.75	0.537	0.741	0.523	0.792	0.698	0.843	0.892	0.714	0.503
2.00	0.503	0.681	0.480	0.726	0.639	0.770	0.814	0.657	0.463

Tab.9.6: Incident waves for Series 60 ($C_B = 0.7$)

As a first computational check, Froude-Krilov forces in head sea are compared with time-domain and strip-method results given by *Beck and Magee (1988)*, Fig.9.9. My RSM results agree well with strip-method results for all force and moment components (in most cases the symbols lie on top each other). For the pitch moment, time-domain results differ somewhat from RSM resp. strip-method results. *Beck and Magee (1988)* do not comment on this discrepancy ("The strip theory and time-domain Froude-Krylov exciting force coefficients are in good agreement for all ships."), but to me it seems that the discrepancies indicate a shortcoming of the time-domain method rather than one of the RSM.

Free-surface grids were created automatically for each wave length. The same grids were used for all Froude numbers and angles of encounter. The grid generation was similar to the stationary case: A rectangular grid is transformed following with its innermost line in a distance $\Delta x/2$ the still water line. Fig.9.10 shows a typical grid created this way. The nomenclature of chapter 7 is used. x_1 denotes the foremost x-value. Each grid consisted of $n_x \cdot n_y = 61 \cdot 15 = 915$ points. The following grid parameters were always the same: $\alpha = 2$, $h_s/\Delta x = 1$. Shifting of collocation points versus source points is done by adding one collocation point at the upstream end and one source point at the downstream end, Fig.9.10. Tab.9.7 lists the variable grid parameters.

λ/L	0.5	0.75	1.0	1.25	1.5	1.75	2.0
x_1 [m]	121.92	152.40	182.88	213.36	243.84	274.32	304.80
Δx [m]	4	5	6	7	8	9	10

Tab.9.7: Variable grid parameters for free-surface grids

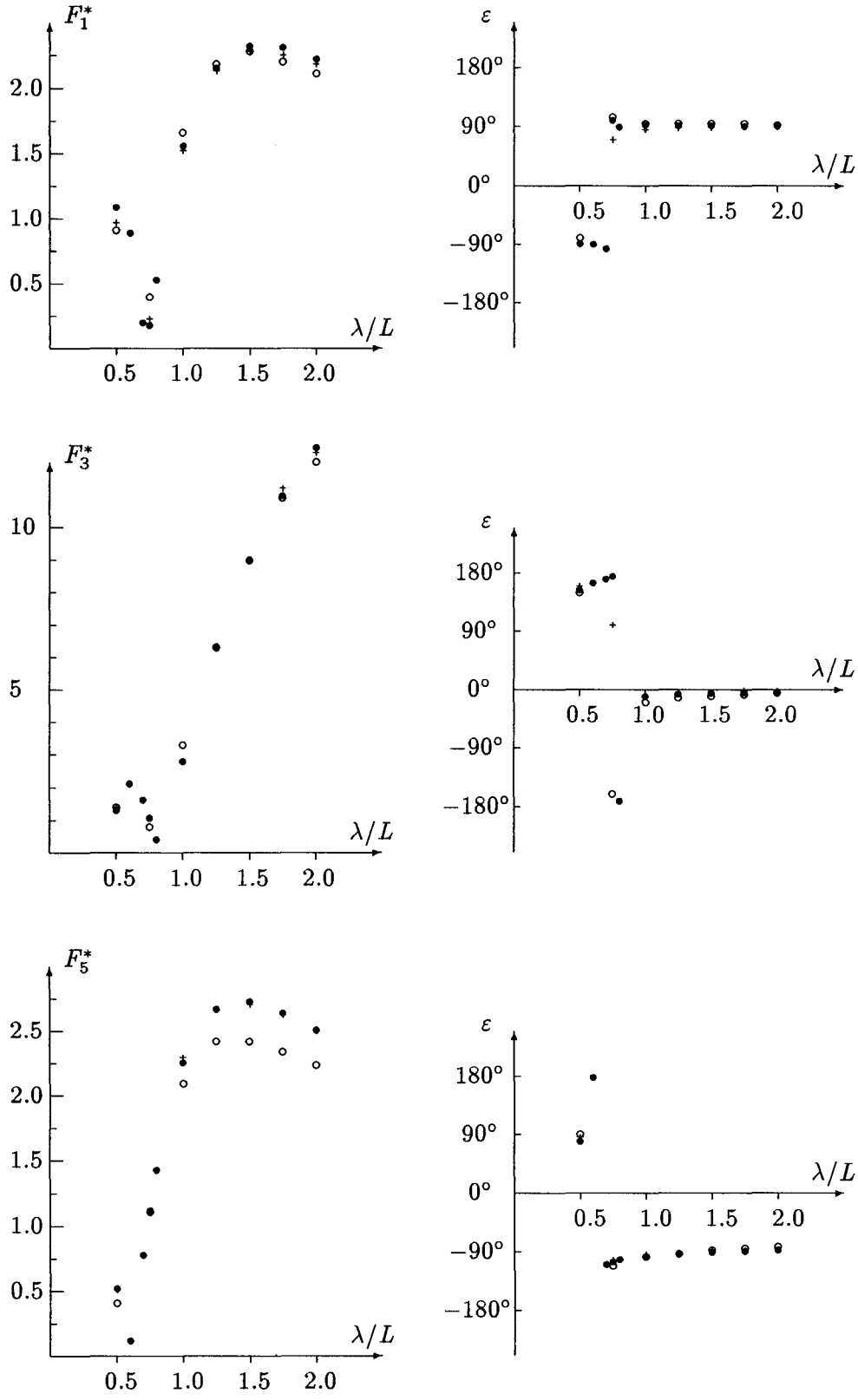

Fig.9.9: Froude-Krilov forces and moments for Series 60, $\mu = 180°$
o time-domain, + strip method, • panel method
$F_1^* = |\hat{F}_1^{fk}|L/\rho g h \nabla$, $F_3^* = |\hat{F}_3^{fk}|L/\rho g h \nabla$, $M_2^* = |\hat{M}_2^{fk}|/\rho g h \nabla$

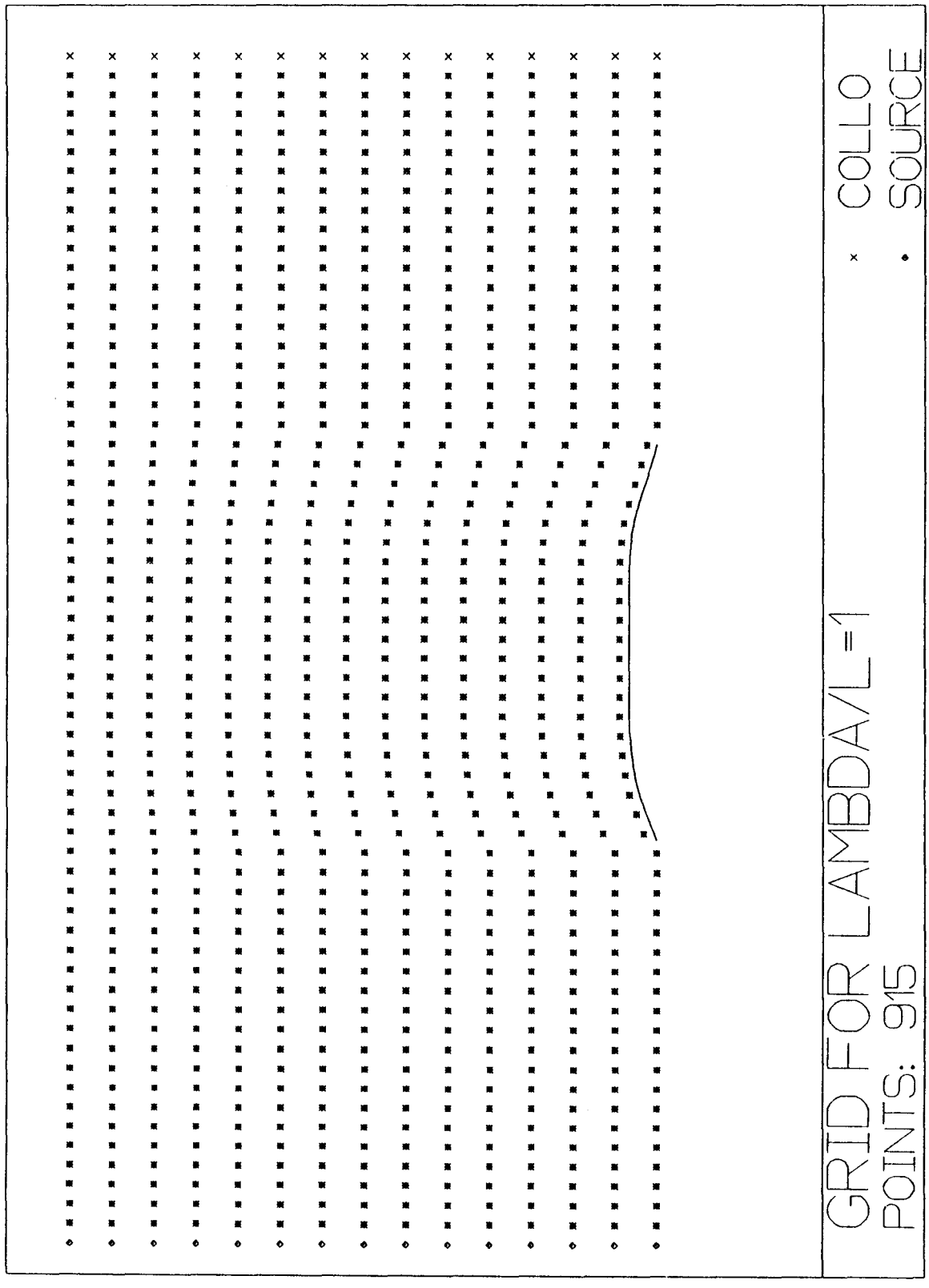

Fig.9.10: Typical free-surface discretization for diffraction problem

For $F_n = 0.2$, $F_n = 0.25$ and $F_n = 0.3$ exciting forces and moments in head sea were calculated using 342 collocation points on the body and 915 on the free surface, Tab.9.8. On a VAX 6310 one λ-F_n-combination needed 106 CPU minutes. It should be noted that solving the system of linear equations (SLE) using a Gauss elimination algorithm required 86% of the CPU time. Straightforward Gauss-Seidel techniques are ruled out by the conditioning of the SLE. Due to the radiation condition, the main diagonal is not dominant. The problem is similar to the stationary case as discussed by *Jensen (1988)*, who also used Gauss elimination. *Jensen et al. (1989)* report on a special SLE-solver consisting of a combination of Gauss elimination and Gauss-Seidel iteration. However, future extension of the program will include solving the radiation problems as well. It is already clear that the boundary conditions for the radiation problems lead to similar SLEs where only the constant vectors resp. right-hand sides are different. CPU-time advantages of the special solver vanish with the increasing number of right-hand sides of the SLE. An adaptation of the special solver from the stationary to the diffraction problem was therefore not considered.

	$F_n = 0.2$						$F_n = 0.25$					
λ/L	F_1^*	ε	F_3^*	ε	M_2^*	ε	F_1^*	ε	F_3^*	ε	M_2^*	ε
0.50	0.98	-77.6	0.84	-157.9	0.49	94.3	1.00	-73.6	1.24	-162.1	0.45	95.2
0.75	0.59	178.4	1.62	-177.9	0.58	-70.5	0.58	-174.9	1.88	-175.0	0.54	-76.1
1.00	1.47	117.1	1.23	37.0	1.58	-78.0	1.49	116.1	0.97	33.4	1.60	-80.9
1.25	1.99	105.2	4.06	19.0	2.04	-80.1	2.06	103.9	3.87	16.3	2.09	-82.2
1.50	2.16	99.5	6.38	14.9	2.20	-81.4	2.26	97.9	6.23	12.9	2.27	-83.6
1.75	2.17	99.6	8.28	13.1	2.20	-82.4	2.28	94.3	8.18	10.7	2.29	-84.4
2.00	2.10	92.7	9.67	11.8	2.14	-83.5	2.24	92.6	9.74	9.8	2.23	-84.0
	$F_n = 0.3$											
λ/L	F_1^*	ε	F_3^*	ε	M_2^*	ε						
0.50	1.10	-78.0	1.25	126.9	0.52	95.6						
0.75	0.61	-165.9	1.98	166.3	0.43	-89.1						
1.00	1.42	115.7	1.05	59.1	1.48	-85.4						
1.25	2.06	101.4	3.53	20.2	2.03	-86.2						
1.50	2.32	95.8	5.99	13.1	2.25	-86.3						
1.75	2.34	92.3	8.08	10.6	2.27	-86.3						
2.00	2.30	90.4	9.66	9.5	2.22	-85.9						

Tab.9.8: Exciting forces for Series 60, $\mu = 180$, phase ε in degree
$F_i^* = |\hat{F}_i^e| L/\rho g h \nabla$, $M_i^* = |\hat{M}_i^e|/\rho g h \nabla$

Fig.9.11 compares results for $F_n = 0.2$ with strip-method and time-domain results of *Beck and Magee (1988)*, experimental results of *Gerritsma (1960)*, and unified-theory results of *Sclavounos (1984)*. For surge exciting forces, RSM agrees well with strip method. Only the phase shows different tendencies in changing from positive to negative values in the vicinity of $\lambda/L = 0.75$. Agreement of time-domain and RSM results is poor. For heave exciting forces, all methods give similar results for longer waves. For the shorter waves, RSM shows the best agreement with experiments. For pitch exciting moments, all methods predict similar phases. The amplitudes show considerable scattering with no method giving good agreement with experiments. Like *Beck and Magee (1988)*, I assumed that *Gerritsma's (1960)* moments relate to a point in the center plane at height of the still-water line. I could not find any explicit confirmation of this assumption. So discrepancies between calculations and experiments might simply be due to a different origin of coordinate systems. RSM agrees well with unified theory and strip method for larger wave lengths.

The number of grid parameters and the relatively high CPU requirement for each grid rule out a systematic investigation of the influence of all grid parameters. Only for the combination $F_n = 0.2$, $\mu = 180°$, and $\lambda/L = 1$ the free-surface grid was varied.

The 3 variations of the standard grid were: (1.) x_1 lies $\Delta x/2$ further aft, (2.) the "optimal" y-shift $\Delta H = 0.02\Delta y$ instead of the standard 0 is used, and (3.) grid spacing $\Delta x = 9$ (instead of 6). Tab.9.9 gives exciting forces and moments obtained with the standard grid and the variations.

grid	F_1^*	ε	F_3^*	ε	M_2^*	ε
standard	1.47	117.1	1.23	37.0	1.58	-78.0
variation 1	1.46	117.1	1.22	36.7	1.58	-78.1
variation 2	1.47	117.1	1.23	37.0	1.58	-78.0
variation 3	1.44	113.3	1.44	47.7	1.60	-81.0

Tab.9.9: Exciting forces for $F_n = 0.2$, $\mu = 180$, $\lambda/L = 1$ for various free-surface grids

As expected, the influence of the first two variations is negligible. The coarser grid – variation 3 – results in a considerably different vertical force. So the standard fine discretization, resulting in high CPU time and storage requirements, is indeed necessary. The changes in the surge force and pitch moment are not significant.

Fig.9.12 compares RSM results for $F_n = 0.25$ with *Gerritsma's (1960)* experiments showing similar agreement as for $F_n = 0.2$.

Fig.9.13 compares RSM results for $F_n = 0.3$ with experiments of *Gerritsma (1960)* and *Gerritsma and Beukelman (1967)*. Experimental models were divided into 7 segments to obtain sectional hydrodynamic coefficients. The experimental values include the sum of the section results in addition to the values for the whole model. For longer waves, RSM results lie in the cluster of experimental results. For the shortest wave length of the experiments ($\lambda = 0.6L$), disagreement is striking. However, only one experimental value is available for this wave. In my opinion the experimental amplitude seems to be implausibly high. Agreement for the next longer wave ($\lambda = 0.75L$) is satisfactory.

In most other diffraction methods, the stationary part of the potential is approximated by uniform parallel flow. I investigated the effect of this simplification: Using the same discretization for ship and free surface, the stationary part of the potential was set to uniform flow, the surface condition applied at $z = 0$, and the pressure integrated up to the still water line. The results are marked by crosses in Fig.9.13. For surge forces the differences are notable. However, for heave and pitch the simplified computation gives similar agreement with experiments as the original one.

Only for the shortest wave ($\lambda/L = 0.5$) the heave exciting force is considerably different. So at least for the Series 60 shape, the additional effort of obtaining the nonlinear solution for the stationary potential does not result in noticable improvements in the region of available experimental data. In this regard, the lack of experimental data for validation in the short-wave range is most unfortunate.

I am not aware of any published results for exciting forces in oblique flow. For $\mu = 150°$ and $F_n = 0.2$, Tab.9.10 and Fig.9.14 give exciting forces and moments without comparison. Behaviour for the symmetrical degrees of freedom (surge, heave and pitch) is similar as for $\mu = 180°$.

λ/L	F_1^*	ε	F_2^*	ε	F_3^*	ε	M_1^*	ε	M_2^*	ε	M_3^*	ε
0.50	0.82	-94.2	1.44	-125.7	1.57	-156.0	0.0109	-107.7	0.23	89.9	0.15	44.6
0.75	1.01	137.4	0.83	27.4	0.60	149.5	0.0129	-63.2	1.05	-70.0	1.04	148.6
1.00	1.78	111.6	2.52	60.1	2.84	26.2	0.0163	-72.0	1.78	-75.8	0.99	161.3
1.25	2.06	102.9	3.25	65.7	5.64	18.7	0.0175	-79.1	2.04	-78.3	0.80	168.5
1.50	2.10	97.7	3.35	71.8	7.72	15.4	0.0170	-78.7	2.08	-80.1	0.61	174.8
1.75	2.03	94.0	3.31	73.6	9.40	13.4	0.0153	-85.3	2.03	-81.3	0.40	178.1
2.00	1.93	91.0	3.11	75.1	10.65	12.2	0.0136	-87.0	1.94	-82.7	0.27	-175.8

Tab.9.10: Exciting forces for Series 60, $\mu = 150$, $F_n = 0.2$, phase ε in degree
$F_i^* = |F_i^*|L/\rho g h \nabla$, $M_i^* = |M_i^*|/\rho g h \nabla$

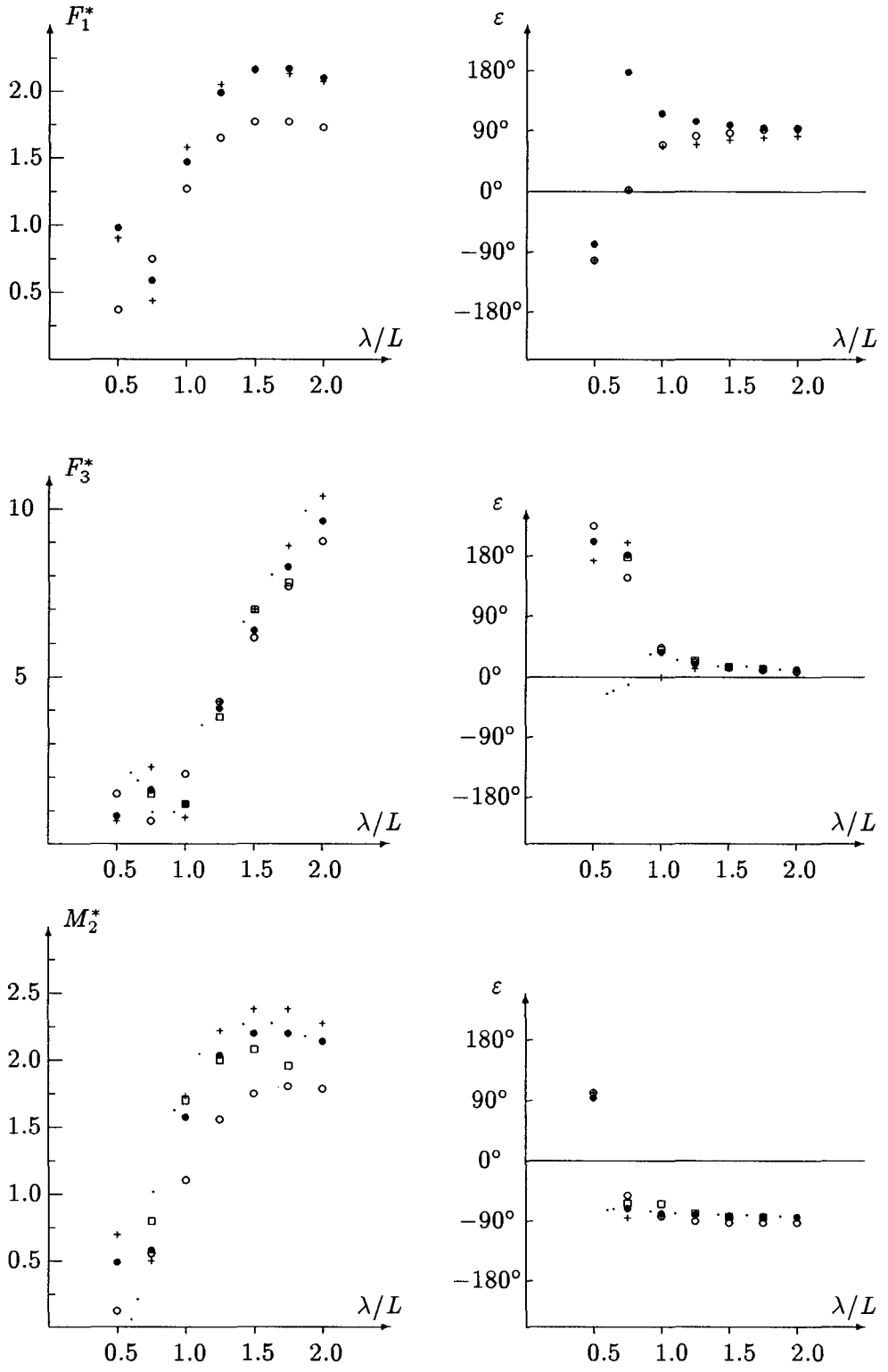

Fig.9.11: Exciting forces and moments for Series 60, $\mu = 180°$, $F_n = 0.2$
o time-domain, + strip method, □ experiment, · unified theory, • panel method
$F_1^* = |\hat{F}_1^e|L/\rho g h \nabla$, $F_3^* = |\hat{F}_3^e|L/\rho g h \nabla$, $M_2^* = |\hat{M}_2^e|/\rho g h \nabla$

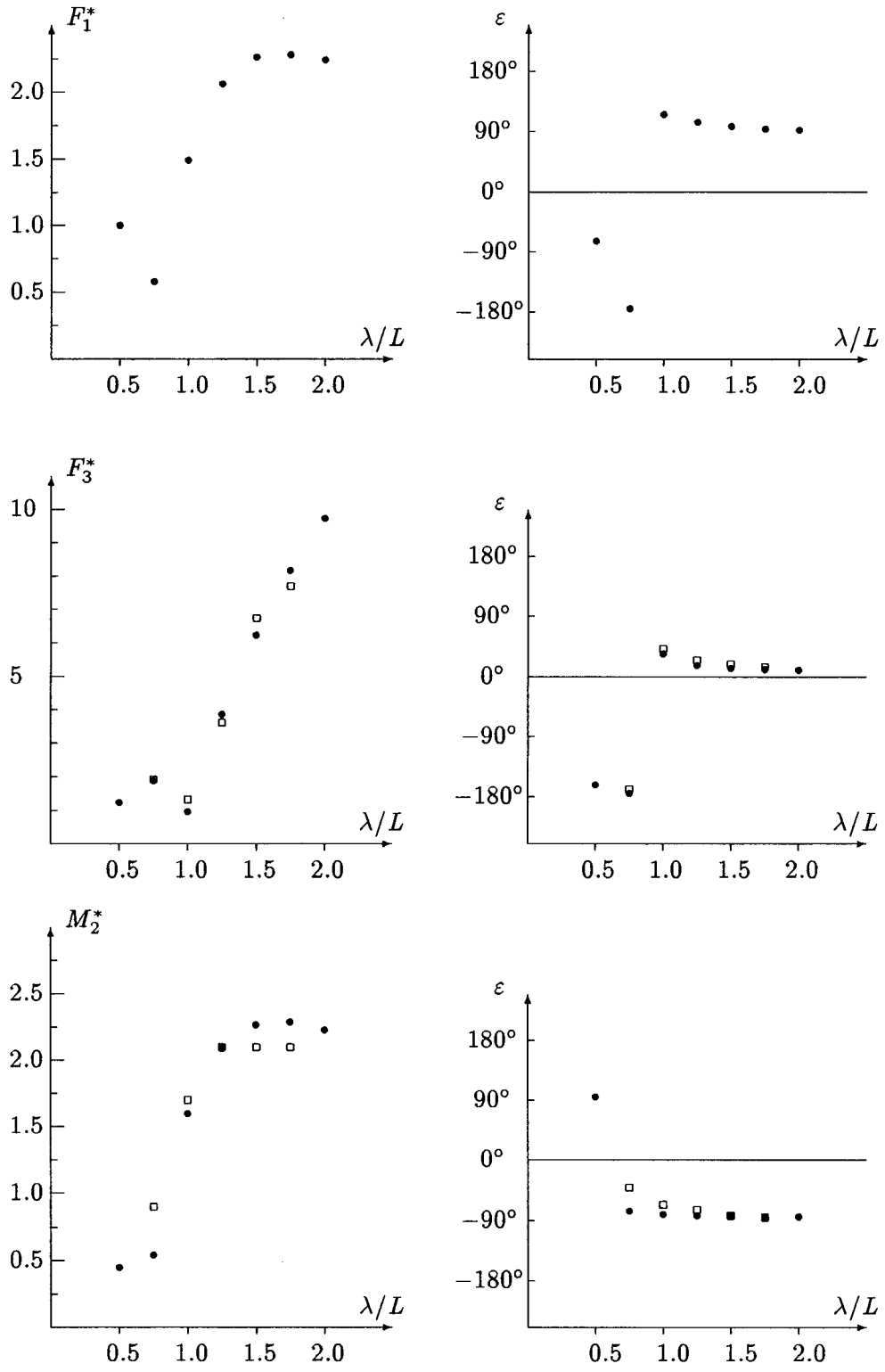

Fig.9.12: Exciting forces and moments for Series 60, $\mu = 180°$, $F_n = 0.25$
□ experiment, • panel method
$F_1^* = |\hat{F}_1^e|L/\rho g h \nabla$, $F_3^* = |\hat{F}_3^e|L/\rho g h \nabla$, $M_2^* = |\hat{M}_2^e|/\rho g h \nabla$

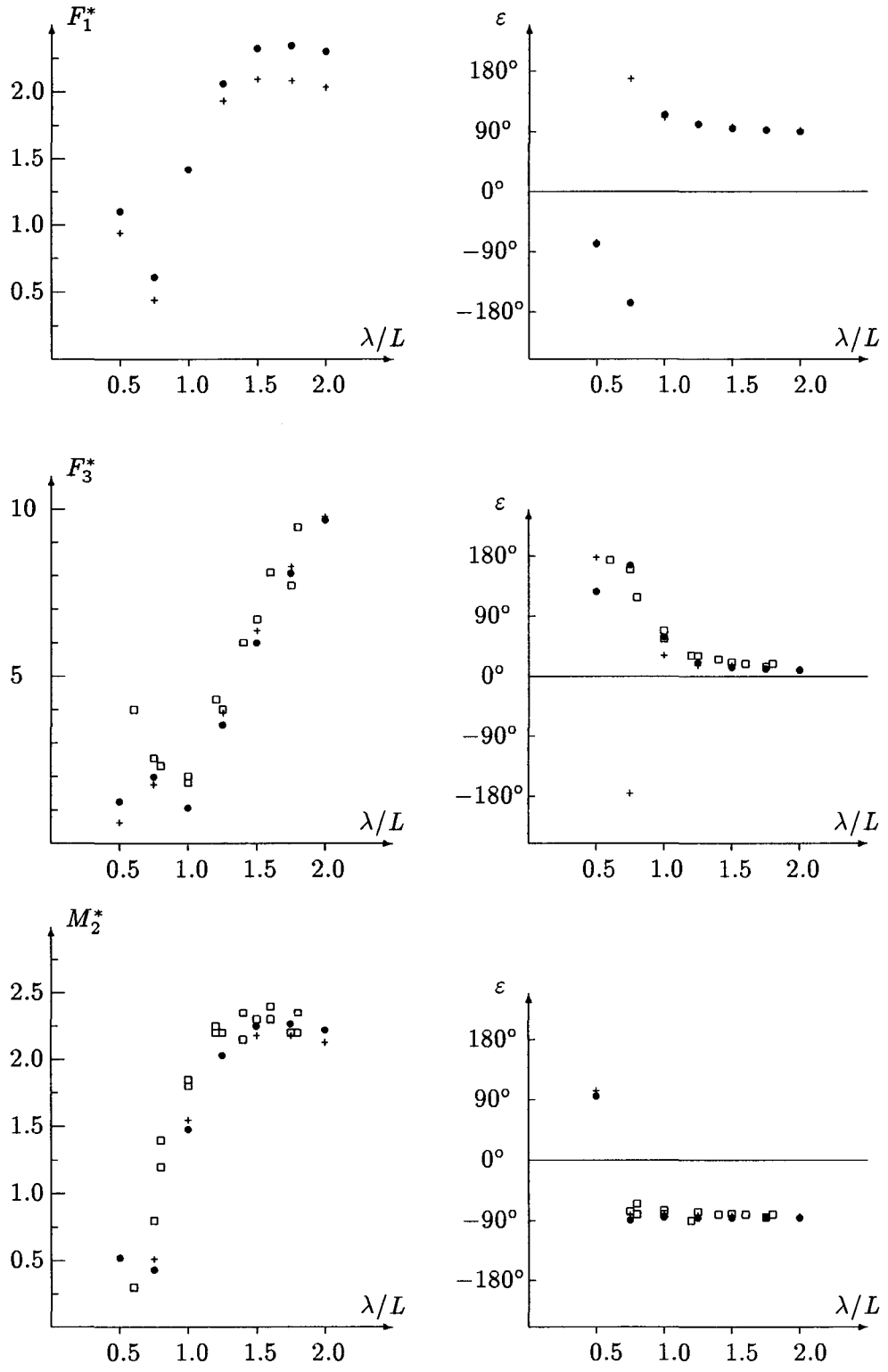

Fig.9.13: Exciting forces and moments for Series 60, $\mu = 180°$, $F_n = 0.3$
□ experiment, • panel method, + simplified panel method
$F_1^* = |\hat{F}_1^e|L/\rho g h \nabla$, $F_3^* = |\hat{F}_3^e|L/\rho g h \nabla$, $M_2^* = |\hat{M}_2^e|/\rho g h \nabla$

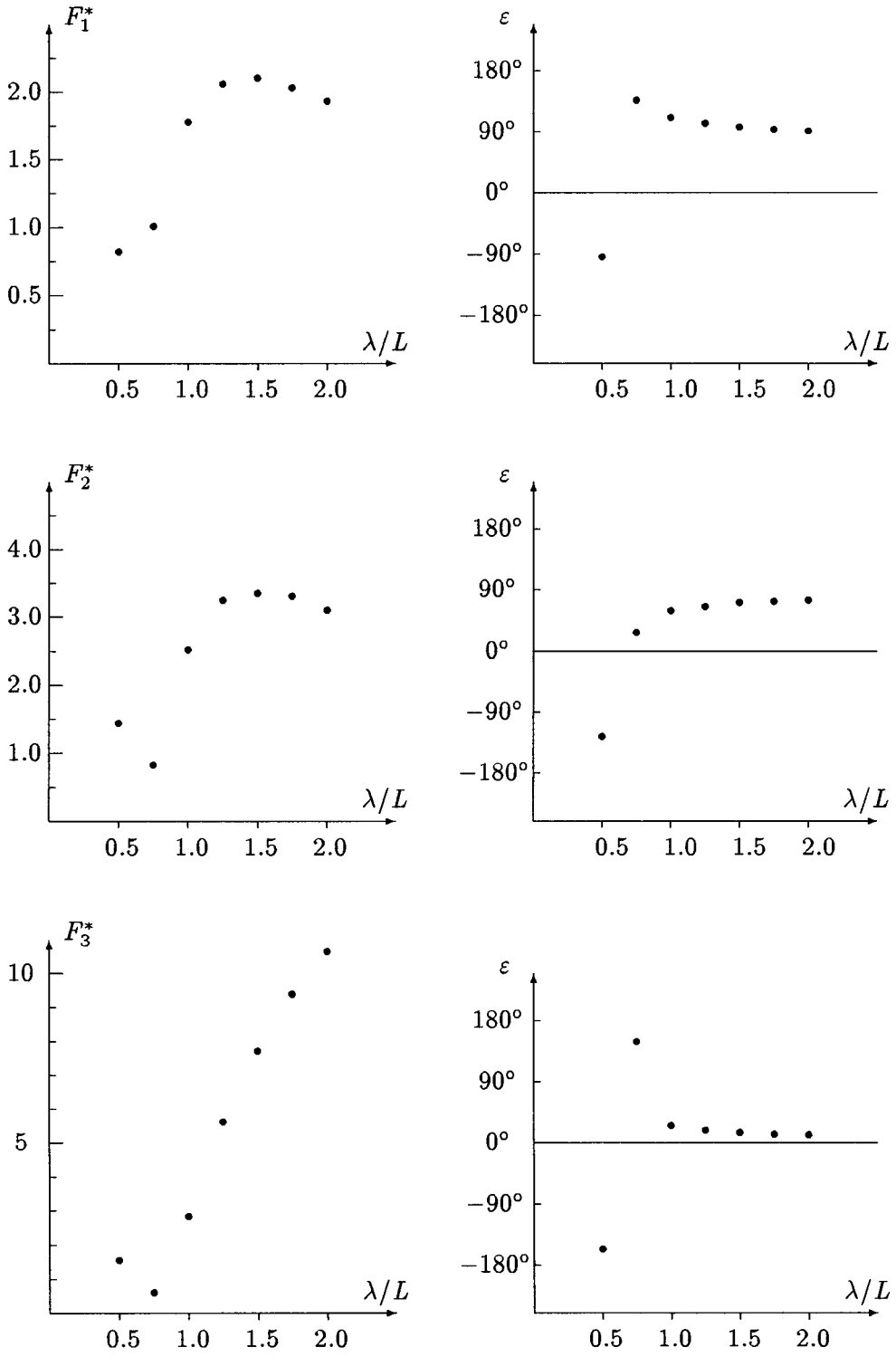

Fig.9.14a: Exciting forces for Series 60, $\mu = 150°$, $F_n = 0.2$
• panel method
$F_1^* = |\hat{F}_1^e|L/\rho g h \nabla$, $F_2^* = |\hat{F}_2^e|L/\rho g h \nabla$, $F_3^* = |\hat{F}_3^e|L/\rho g h \nabla$,

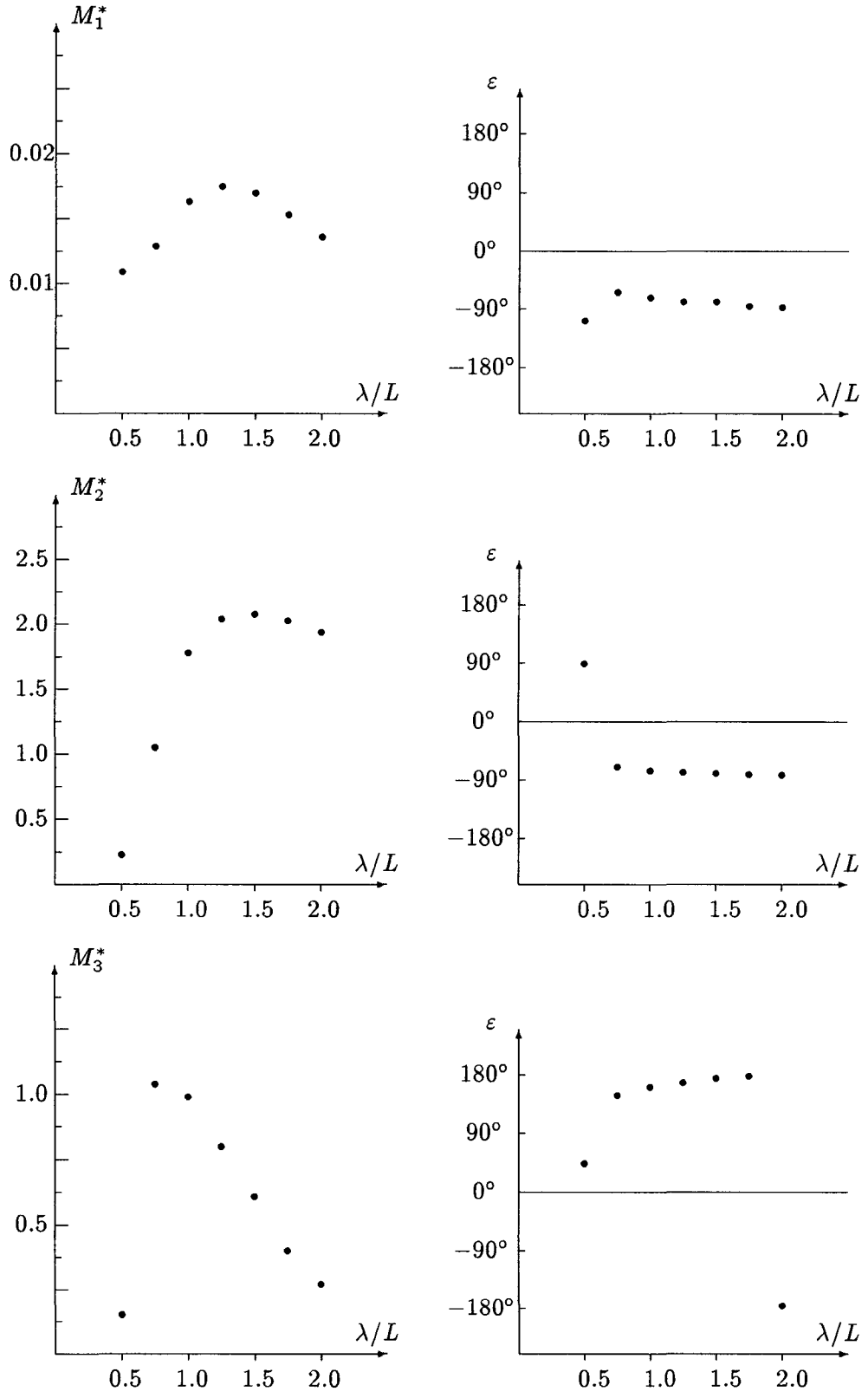

Fig.9.14b: Exciting moments for Series 60, $\mu = 150°$, $F_n = 0.2$
• panel method
$M_1^* = |\hat{M}_1^e|/\rho g h \nabla$, $M_2^* = |\hat{M}_2^e|/\rho g h \nabla$, $M_3^* = |\hat{M}_3^e|/\rho g h \nabla$,

10. Conclusion

The forward-speed diffraction problem for $\tau = U\omega_e/g > 0.25$ is solved in a Rankine source method. Potential flow is assumed. First the stationary part of the potential is determined in a Rankine source method meeting the nonlinear free-surface boundary condition. The potential of the incident wave of small amplitude is known. A Rankine source distribution approximates the remaining diffraction potential. The boundary conditions at the free surface and the ship hull are fulfilled in a collocation scheme. Radiation and open-boundary condition are enforced by shifting sources versus collocation points.

The method is applied to a submerged spheroid and a Series 60 parent form ($C_B = 0.7$). Good agreement with other computational methods and experiments is found. However, it is found that the usual approximation for the stationary part of the flow by uniform flow does not lead to significantly different results. CPU time and storage requirements are dominated by the system of linear equations (SLE) for determining the source strength distribution. In view of future development of the programs, use of a different SLE-solver does not seem worthwile. It remains to be seen whether an extension to the radiation problems and determination of motions will show substantial improvements over the strip method. Furthermore, reliable experimental data for short and oblique waves are needed for proper validation of the computational results.

References

R.F. BECK, L.J. DOCTORS (1987)
Convergence properties of the Neumann-Kelvin problem for a submerged body
Journal of Ship Research Vol.31/4

R.F. BECK, A. MAGEE (1988)
Compendium of ship motion calculations using linear time-domain analysis
Univ. of Michigan, Dept. of NA&ME Rep. 310

V. BERTRAM (1990)
Fulfilling open-boundary and radiation condition in free-surface problems using Rankine sources
Ship Technology Research Vol. 37/2

V. BERTRAM, G. JENSEN (1987)
Numerische Berechnung des Schiffswellenwiderstands
IfS-Report 477, Univ. Hamburg

Y. CAO, W.W. SCHULTZ, R.F. BECK (1989)
Numerical investigation on the desingularization of boundary integral equation for three-dimensional nonlinear wave problems
4th Int. Workshop on Floating Bodies and Water Waves, Øystese

Y. CAO, W.W. SCHULTZ, R.F. BECK (1990)
Three-dimensional desingularized boundary integral methods for potential problems
Univ. of Michigan, Techn. Rep. 89-09

M.S. CHANG (1980)
Computations of three-dimensional ship-motions with forward speed
2nd Int. Conf. on Num. Ship Hydrodyn., Berkeley

O. FALTINSEN (1987)
Numerical techniques in seakeeping
18th ITTC Conf., Kobe

J. GERRITSMA (1960)
Shipmotions in longitudinal waves
I.S.P. Vol.7

J. GERRITSMA, W. BEUKELMAN (1967)
Analysis of the modified strip theory for the calculation of ship motions and wave bending moments
Rep. Nr. 96S, Netherlands Ship Research Centre TNO, Delft

S.A. HARVALD (1983)
Resistance and propulsion of ships
John Wiley&Sons

J. HESS, A.M.O. SMITH (1964)
Calculation of nonlifting potential flow about arbitrary three-dimensional bodies
Journal of Ship Research Vol.8/2

R.B. INGLIS, W.G. PRICE (1981)
The influence of speed dependent boundary conditions in three dimensional ship motion problems
I.S.P. Vol.28

G. JENSEN (1988)
Berechnung der stationären Potentialströmung um ein Schiff unter Berücksichtigung der nichtlinearen Randbedingung an der Wasseroberfläche
IfS-Report 484, Univ. Hamburg

G. JENSEN, V. BERTRAM, H. SÖDING (1989)
Numerical determination of non-linear free surface flows around ships
5th Int. Conf. on Num. Ship Hydrodyn., Hiroshima

G. JENSEN , Z.-X. MI, H.SÖDING (1986)
Rankine Source Methods for Numerical Solutions of the Steady Wave Resistance Problem
16th Symp. Nav. Hydrodyn., Berkeley

B. KING (1987)
Time-domain analysis of wave exciting forces on ships and bodies
Univ. Michigan, Dept. of NA&ME Rep. 304

B.V. KORVIN-KROUKOVSKY (1955)
Investigation of ship motions in regular waves
Trans. SNAME, 63

B.V. KORVIN-KROUKOVSKY, W.R. JACOBS (1957)
Pitching and heaving motions of a ship in regular waves
Trans. SNAME, 65

K.-Y. LEE (1983)
Widerstandserhöhung in kurzen Wellen
Schiffstechnik Vol.30/3

S.J. LIAPIS (1986)
Time-domain analysis of ship motions
Dissertation, Univ. of Michigan

S.J. LIAPIS, R.F. BECK (1985)
Seakeeping computations using time-domain analysis
4th Int. Conf. on Num. Ship Hydrodyn., Washington

D.E. NAKOS (1989)
Free surface panel methods for unsteady forward speed flows
4th Int. Workshop on Floating Bodies and Water Waves, Øystese

D.E. NAKOS, P.D. SCLAVOUNOS (1990)
Ship wave patterns
Journal of Fluid Mechanics, Vol.209

J.N. NEWMAN (1978)
The theory of ship motions
Adv. Appl. Mech. Vol.18

M. OHKUSU, H. IWASHITA (1989)
Evaluation of the Green function for ship motions at forward speed and application to radiation and diffraction problems
4th Int. Workshop on water waves and floating bodies, Øystese

I. ORLANSKI (1976)
A simple boundary condition for unbounded hyperbolic flows
Journal of Computational Physics No.21

N. SALVESEN, E.O. TUCK, O. FALTINSEN (1970)
Ship motions and sea loads
Trans. SNAME, 78

W.W. SCHULTZ, Y. CAO, R.F. BECK (1990)
Three-dimensional nonlinear wave computation by desingularized boundary integral method
5th Int. Workshop on water waves and floating bodies, Manchester

H. SCHULZE (1969)
Eine dreidimensionale Singularitäten-Methode zur Berechnung der oszillierenden hydrodynamischen Größen für die gekoppelte Tauch- und Stampfschwingung eines fahrenden Schiffes in einer ebenen längslaufenden Welle
IfS-Report 261, Univ. Hamburg

P.D. SCLAVOUNOS (1984)
The unified slender-body theory: ship motions in waves
15th Symp. on Nav. Hydrodyn., Hamburg

P.D. SCLAVOUNOS, D.E. NAKOS (1988)
Stability analysis of panel methods for free surface flows with forward speed
17th Symp. on Nav. Hydrodyn., The Hague

H. SÖDING (1979)
Routinen zur Interpolation, Integration und Optimierung
ESS-Report Nr.33, Lehrstuhl und Institut für Entwerfen von Schiffen und Schiffstheorie, TU Hannover

H. SÖDING, E. GERLACH (1987)
Benutzerhandbuch für das Programm EUMEDES
IfS-Script Nr. 2362, Univ. Hamburg

SÖDING, H., TONGUC, E. (1989)
Archimedes II – A program for evaluating hydrostatics and space utilization in ships and offshore structures
Ship Technology Research Vol. 36/2

F.H. TODD (1953)
Some further experiments on single screw merchant ship forms - Series Sixty
SNAME

F.H. TODD (1963)
Series 60 – Methodical experiments with models of single-screw merchant ships
David Taylor Model Basin Report 1712

W.C. WEBSTER (1975)
The flow about arbitrary three-dimensional smooth bodies
Journal of Ship Research Vol.19/4

J.V. WEHAUSEN, E.V. LAITONE (1960)
Handbuch der Physik, Vol.9
Springer-Verlag, Berlin

R.W. YEUNG, K.J. BAI (1974)
Numerical solutions to free surface problems
10th Symp. Nav. Hydrodyn., MIT

R.W. YEUNG, S.H. KIM (1981)
Radiation forces on a ship with forward speed
3rd Int. Conf. on Num. Ship Hydrodyn., Paris

Y. ZHOU (1988)
Beschreibung des Programmsystems BUEF6G
IfS-Report 485, Univ. Hamburg

"Irrational persistence can be a powerful force"

Tidings, *W. Wharton*